Mineralogy and Petrology (2007) 89: 159–188
DOI 10.1007/s00710-006-0141-9
Printed in The Netherlands

Mineralogy and Petrology

Distribution and mineralogy of platinum-group elements in altered chromitites of the Campo Formoso layered intrusion (Bahia State, Brazil): control by magmatic and hydrothermal processes

G. Garuti[1], **J. A. Proenza**[2], and **F. Zaccarini**[3]

[1] University of Modena and Reggio Emilia, Italy
[2] University of Barcelona, Spain
[3] University of Leoben, Austria

Received December 13, 2005; accepted March 30, 2006
Published online November 9, 2006;
Editorial handling: J. G. Raith

Summary

Polyphase, penetrative hydrothermal metasomatism in chromitites of the Campo Formoso layered intrusion produced spectacular chromite – ferrian chromite zoning and transformed the primary intercumulus silicates into a chlorite – serpentine – carbonate – talc assemblage. Alteration did not substantially modify the composition of chromite cores and the distribution of platinum-group elements (PGE) through the sequence of chromitite layers, which still are consistent with magmatic fractionation processes. Texture and composition of laurite and Os–Ir–Ru alloys included in chromite cores indicate that these PGM were not altered, and are probably magmatic in origin. In contrast, the PGM located in the intergranular chlorite matrix (laurite, Ir–Ru–Rh sulfarsenides and Pt–Pd compounds with Sb, Bi and Te) display evidence of hydrothermal reworking. These PGM are intimately intergrown with low-temperature Ni-sulfides. The paragenesis suggests that the Ni-sulfides-PGM assemblage formed at the expenses of unknown PGM precursors, which must have been originally present in the intercumulus silicate matrix. Mechanism of formation involves a sequence of dissolution-precipitation events controlled by variation of redox conditions during chromite alteration. The presence of a secondary ore mineral assemblage consisting of galena, bismuthinite, native antimony, and various Pb–Sb compounds suggests a possible contribution of fluids derived from the adjacent granite.

Introduction

The platinum group elements (PGE) have traditionally been considered to be inert during low-temperature alteration, and practically immobile under hydrothermal conditions, being transported and concentrated mainly by magmatic processes. The chondritic patterns of a number of serpentinized mantle peridotites apparently confirm this conclusion. Since the last three decades, however, the noble behavior of the PGE and their geochemical immobility have been more and more questioned by the discovery in nature of platinum group mineral (PGM) sulfides, alloys and oxides unequivocally crystallized at temperatures much lower than magmatic (*Stumpfl*, 1974). Among the various examples reported in the literature, one of the most prominent ones are ''chromitites'' associated with igneous mafic-ultramafic complexes. Chromian spinel from chromitites commonly contains discrete inclusions of PGM which are interpreted as early liquidus phases entrapped during crystallization of the host phase at magmatic temperatures (*Augé*, 1985, 1987, 1988; *Augé* and *Johan*, 1988; *Constantinides* et al., 1980; *Garuti* et al., 1999; *Melcher* et al., 1997; *Talkington* et al., 1984). Furthermore PGM can be present interstitial to chromite, usually associated with intercumulus magmatic sulfides. Recent studies have proven that these primary PGM may become unstable during alteration of the host rocks, providing the source material for the crystallization of secondary PGM, by the interaction with relatively cool hydrothermal solutions (*Stockman* and *Hlava*, 1984; *Ferrario* and *Garuti*, 1988; *Prichard* et al., 1994; *Garuti* and *Zaccarini*, 1997; *Garuti* et al., 1997; *Zaccarini* et al., 2005b). Although bulk-rock PGE ratios may remain unchanged in most cases, indicating migration of the PGE over short distance, the mineralogical nature of the PGM can be drastically modified, giving rise to assemblages containing newly formed phases which become stable at low temperature.

The Campo Formoso layered intrusion of Brazil provides a useful example for studying these low temperature processes. The complex contains a sequence of chromitite layers hosted in highly serpentinized and chloritized ultramafic rocks. Recently, *Lord* et al. (2004) have reported on the chromite chemistry and PGE distribution in chromitite layers from one of the deposits of Campo Formoso (Cascabullhos), and emphasized the similarity of the fractionation patterns observed at this locality with those of chromitite layers in the Bushveld complex of South Africa. Although the PGE geochemistry reflects igneous fractionation, preliminary description of PGM in the chromitites (*Garuti*, 1991) indicated the possible existence of two genetically different populations, one crystallized in the magmatic stage, the other tentatively interpreted as formed by remobilzation of PGE under hydrothermal conditions.

In this paper, we report the results of a detailed study of chromite composition, PGE abundance and PGM mineralogy in chromitite from four different cross sections exposed in the mines of Cascabulhos, Pedrinhas, Limoeiro, and Mato Limpo. The principal aim of this investigation was to highlight the relative roles of igneous fractionation and post-magmatic alteration processes as factors controlling the distribution and mineralogy of the PGE.

Geological and petrological background

The Campo Formoso layered intrusion (Fig. 1A) is located about 400 km NW of Salvador (Bahia State), in the northern part of the São Francisco craton at about

10° 40′ Latitude South and 40° 20′ Longitude West. The complex consists of a tabular, arch-shaped body approximately 40 km long and 100–1100 m wide, and dipping 52–68° SE (*Ferreira* et al., 2003). The base of the layered sequence is probably exposed at the south western edge of the intrusion, at the base of the Cascabulhos section (*de Deus* et al., 1982), where igneous rocks are overlying Archean granulites of the Caraíba Group (3.0–2.5 Ga). The original thickness of the igneous sequence is unknown due to deep erosion of the upper portion of layers, so that the ultramafic rocks are in contact with Early Proterozoic quartzites of the Jacobina Group, in which thin horizons of detrital chromite are found. During the Transamazonic deformation event (2.2–1.8 Ga), the layered complex underwent low-grade regional metamorphism and was intruded by granites (2.0 Ga) that produced further metasomatism of both igneous and sedimentary rocks (*de Deus* et al., 1982). Late injection of diabase dikes conclude the geological cycle of the Campo Formoso complex.

As a consequence of this long geological history, almost no relic of the primary igneous lithology of the Campo Formoso intrusion was preserved. However, based on bulk-rock geochemistry of altered ultramafic rocks at Cascabulhos, *Lord* et al. (2004) were able to establish that the currently-exposed cross section originally consisted of peridotite in the first 400–500 meters, and of pyroxenite further upwards.

The alteration process of ultramafic rocks of Campo Formoso has been described in detail by *Boukili* et al. (1983). According to these authors a first stage of serpentinization, associated with the regional metamorphism, transformed the ultramafic rocks into a lizardite-chrysotile-magnetite-bastite assemblage. During a second stage, the lizardite-chrysotile-chromite assemblage was replaced by various generations of chlorite and antigorite, while abundant chromian clinochlore developed in chromite rich zones of the complex. The third stage is characterized by carbonatization, steatitization and silicification, by which the chlorite-rich assemblages were replaced by magnesite, talc, dolomite, calcite and quartz, and the rare Cr-bearing hydroxycarbonates stictite and barbertonite (*Boukili* et al., 1984; *Calas* et al., 1984). Sometimes, talc is replaced by magnesite that in turn can be resilicified to form late-generation talc, as a result of the migration of the carbonatization-steatitization boundary through the altered rocks. Recently, *Zaccarini* et al. (2005a) have reported the occurrence of monazite-(La), monazite-(Ce), apatite, galena, bismuthinite, antimony, and unknown Pb–Sb compounds from chromitite samples, and have suggested that La, Ce, P, Pb, Bi and Sb were metasomatically added to the Campo Formoso chromitite horizons by fluids emanating from the nearby Campo Formoso calc-alkaline batholith as it cooled. Based on the mineralogical assemblage of secondary minerals, *Boukili* et al. (1984) inferred temperatures lower than 400–350 °C for the chloritization event at Campo Formoso. Chlorite geothermometry apparently confirms this assumption giving a temperature range of 200–300 °C for the crystallization of chlorite (*Zaccarini* et al., 2005a).

Analytical methods

A total of 66 chromitite samples were collected at the mining localities of Cascabulhos (32), Pedrinhas (10), Limoeiro (14), and Mato Limpo (10) (Fig. 1).

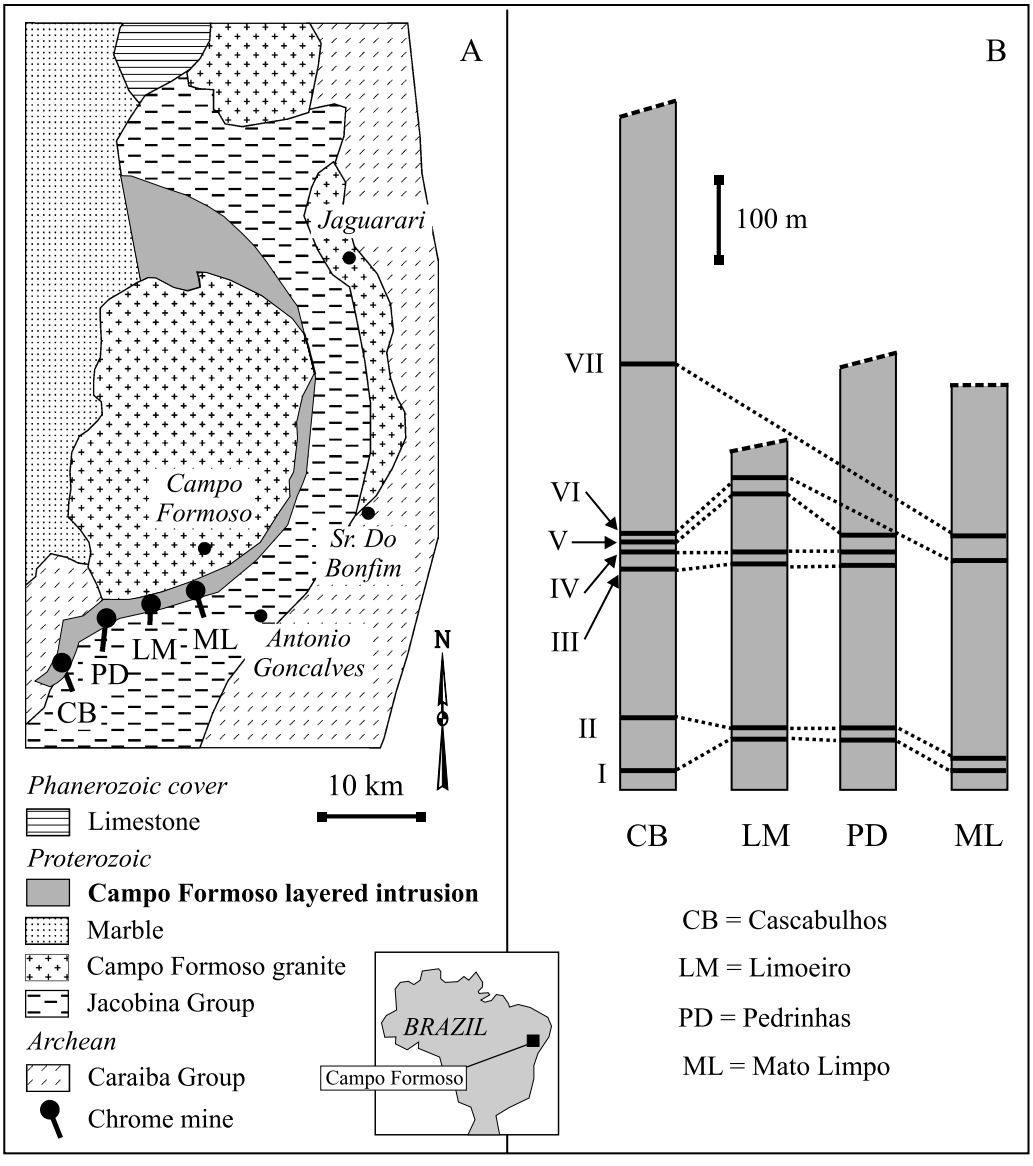

Fig. 1. **A** Geographic location and simplified geological map of the Campo Formoso complex (Bahia State, Brazil). **B** Stratigraphic correlation of major chromitite layers across four mine sections at the investigated localities (modified after *de Deus* et al., 1982)

The petrography and mineralogy of the samples were investigated on 124 polished blocks and polished thin sections by both optical and electronic microscopy and by electron microprobe analysis. The SEM images and chemical analyses of silicates, sulfides and PGMs were performed at the Modena University, using a Philips 515 scanning electron microscope and an ARL-SEMQ electron microprobe, respectively. Details of operating conditions and detection limits are reported in *Garuti* and *Zaccarini* (1997), *Zaccarini* et al. (2004, 2005b) and references therein.

Total PGE concentrations were determined by Ni sulfide fire assay and ICP-MS at XRAL laboratories (Don Mills, Ontario, Canada). Selected samples

were also analyzed by the same method at the Universities of Modena and Reggio Emilia (Italy) and Granada (Spain). Detection limits for the last set of analyses were as follows: 0.5 ppb for Os and Ru, and 0.1 ppb for Ir, Rh, Pt and Pd.

The Campo Formoso chromitites

Stratigraphy and petrography

The sequence of chromitite layers hosted in the Campo Formoso layered intrusion represents one of the most prominent chromite deposits of Brazil. The total inferred reserves amount to about 36 millions metric tons of combined lump (massive), stratified (layered) and disseminated chromite ore varying from 15–20% to 30–45% Cr_2O_3 (*de Deus* et al., 1982). Chromitites occur as a succession of layers and lenses extending over several hundreds of meters and varying in thickness from a few centimeters up to 15 meters. Reconstruction of the original stratigraphy is problematic due to intensive faulting and deformation. However, based on variations in ore texture, thickness of layers and bulk-ore geochemistry, *de Deus* et al. (1982) established a correlation among three different cross sections at Cascabulhos, Pedrinhas and Limoeiro (Fig. 1B). The most complete stratigraphy (∼900 m) is exposed at Cascabulhos, where 7 chromitite layers have been recognized (11 according to *Lord* et al., 2004), three of which (No. IV, V, VI) contain the largest chromite reserves. The sections of Pedrinhas (∼600 m) and Limoeiro (∼450 m) cut across the successions of layers No. III–V and No. IV–VI, respectively. However, at the time of sampling for this study in 1988, the occurrence of a lower group of layers, possibly attributable to No. I and II, had already been established by mining exploration at both localities.

The samples examined in this study represent different types of chromite ore, varying from massive, to high-grade disseminated, and layered or stratified chromitite. With the exception of samples from the Pedrinhas mine which contain serpentine as the major interstitial silicate, chromian clinochlore is the main gangue mineral. Subordinate amounts of talc, magnesite, dolomite and calcite occur as irregular patches replacing the chlorite matrix. Microscopic veins and fissures filled with dolomite and calcite are visible in several chromitites on the hand-specimen scale. Samples characterized by the lizardite-chrysotile-magnetite assemblage show weak or no ferrian chromite alteration, and a cumulus texture is locally preserved (Fig. 2A). In most samples, however, the original texture has been modified by significant alteration of the chromite, as exemplified by a complex zoning; unaltered chromite occurs within the core of partially altered grains and is replaced by a higher reflective spinel phase (ferrian chromite) along rims and cracks. This replacement is also observed inside some grains, around inclusions of secondary chlorite (Fig. 2B). With proceeding alteration the ferrian chromite becomes porous and intimately intergrown with chromian clinochlore and carbonates (Fig. 2C). The shape of chromite grains becomes rounded due to chemical dissolution of the ferrian chromite, and the grains loose their original euhedral shape. The hydroxy-carbonate stichtite was observed in several samples at the rim of chromite grains, usually replacing porous ferrian chromite.

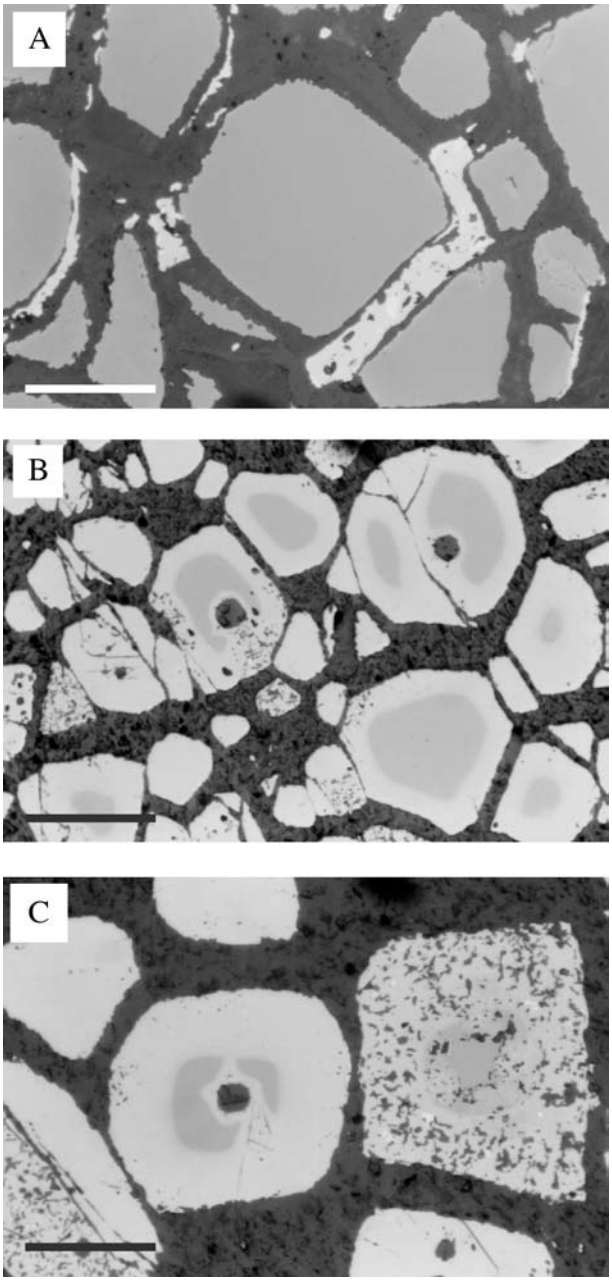

Fig. 2. **A** Unaltered chromite grains rimmed by secondary magnetite formed during serpentinization of intercumulus olivine (Pedrinhas mine). **B** Moderately altered chromite grains in strongly chloritized chromitite (Cascabulhos mine): unaltered chromite (dark core) is replaced by compact ferrian chromite of first generation (light gray rim) and spongy ferrian chromite of second generation (spotted light gray rim). **C** Strongly altered chromite grains in chromitite with carbonate veins (Cascabulhos mine): compact ferrian chromite is almost totally replaced by spongy ferrian chromite intimately intermixed with chromian clinochlore, dolomite and magnesite. Reflected light microphotographs, dark gray = silicate-carbonate matrix, middle gray = chromite, light gray = ferrian chromite. Scale bar = 0.25 mm

Chromite composition

Electron microprobe compositions of cores of chromite grains (Table 1) define trends of decreasing #Cr [$= Cr/(Cr + Al)$], and increase of both TiO_2 and $\#Fe^{3+}$ [$= Fe^{3+}/(Fe^{3+} + Cr + Al)$] with increasing $\#Fe^{2+}$ [$= Fe^{2+}/(Fe^{2+} + Mg)$] ratio (Fig. 3). There is an extensive overlap of compositions among chromites of layers III–V in each locality. However, layers I and II are characterized by higher #Cr and lower $\#Fe^{2+}$, Ti, Fe^{3+} and total Fe, compared to chromitites in the higher stratigraphic levels (VI and VII), which plot at the opposite end of the trend. Our

Table 1. *Selected electron microprobe composition of chromite cores from chromitite layers of the Campo Formoso layered intrusion*

Locality/ layer	Ore type	SiO_2	TiO_2	Al_2O_3	FeO	Fe_2O_3	MgO	MnO	Cr_2O_3	NiO	Total	$\#Fe^{2+}$	#Cr
Cascabulhos													
I	massive	0.33	0.15	13.63	20.42	5.05	9.02	0.26	50.64	0.11	99.61	0.69	0.71
I	disseminated	0.34	0.25	15.28	19.22	4.02	10.19	0.25	50.68	0.16	100.39	0.65	0.69
II	massive	0.33	0.20	14.78	19.02	3.77	10.07	0.36	51.12	0.09	99.74	0.65	0.70
III	massive	0.29	0.22	17.61	22.65	5.32	8.11	0.38	45.82	0.06	100.46	0.73	0.64
IV	massive	0.33	0.19	15.65	19.63	4.46	9.99	0.55	50.58	0.08	101.46	0.66	0.68
IV	stratified	0.00	0.23	14.13	18.88	5.54	9.91	0.66	51.63	0.05	101.03	0.65	0.71
V	massive	0.00	0.20	15.18	18.79	4.18	9.98	0.49	51.14	0.05	100.00	0.65	0.69
VI	massive	0.00	0.21	15.50	21.90	3.34	8.17	0.54	51.50	0.14	101.30	0.73	0.69
VI	disseminated	0.00	0.13	10.95	24.55	8.28	6.04	0.45	51.19	0.10	101.69	0.80	0.76
VII	massive	0.20	0.32	19.76	21.21	5.87	9.33	0.19	43.39	0.09	100.36	0.69	0.60
VII	massive	0.20	0.31	19.51	23.24	6.19	7.80	0.19	42.15	0.15	99.74	0.75	0.59
VII	accessory	0.32	0.36	10.64	29.50	6.89	2.96	0.22	48.66	0.01	99.56	0.91	0.75
VII	accessory	0.22	0.39	17.87	28.11	8.01	4.39	0.22	39.77	0.06	99.04	0.86	0.60
Pedrinhas													
I	stratified	0.05	0.19	11.94	12.71	3.32	13.69	0.18	57.13	0.08	99.29	0.48	0.76
II	disseminated	0.03	0.20	15.04	13.55	4.04	13.61	0.19	53.46	0.11	100.23	0.50	0.70
II	massive	0.07	0.18	11.56	13.35	3.21	13.08	0.21	56.93	0.12	98.71	0.50	0.77
III	massive	0.10	0.20	15.24	14.66	3.27	13.00	0.20	53.48	0.05	100.20	0.53	0.70
III	disseminated	0.06	0.17	13.96	13.96	2.29	13.13	0.21	55.74	0.09	99.61	0.51	0.73
IV	massive	0.06	0.18	15.23	15.79	2.65	12.10	0.20	53.46	0.10	99.77	0.56	0.70
IV	massive	0.04	0.17	13.73	14.87	2.45	12.72	0.28	56.52	0.07	100.85	0.54	0.73
V	stratified	0.08	0.17	12.70	17.44	3.71	10.77	0.22	54.61	0.07	99.77	0.62	0.74
Limoeiro													
I	massive	0.11	0.20	12.19	17.53	3.45	10.74	0.51	56.07	0.08	100.88	0.62	0.76
II	massive	0.17	0.16	11.89	17.16	3.39	10.76	0.49	55.55	0.02	99.59	0.61	0.76
III	massive	0.04	0.17	13.99	12.98	4.64	13.65	0.46	54.05	0.12	100.10	0.48	0.72
IV	massive	0.15	0.19	14.35	18.56	3.89	10.11	0.46	51.87	0.03	99.61	0.64	0.71
IV	disseminated	0.11	0.21	14.04	20.35	6.54	9.05	0.44	49.81	0.09	100.64	0.69	0.70
V	disseminated	0.13	0.18	14.26	18.98	4.72	9.77	0.43	51.09	0.13	99.69	0.66	0.71
VI	massive	0.11	0.14	13.98	23.46	7.51	6.86	0.66	48.06	0.10	100.88	0.77	0.70
VI	top-mass	0.08	0.15	14.50	22.36	7.26	7.83	0.61	48.78	0.06	101.63	0.74	0.69
Mato Limpo													
I	massive	0.09	0.16	14.24	15.79	3.11	11.93	0.38	54.16	0.10	99.96	0.57	0.72
II	stratified	0.02	0.15	14.20	15.65	2.40	11.83	0.43	54.82	0.15	99.65	0.57	0.72
III	stratified	0.11	0.18	14.59	16.50	2.95	11.58	0.41	53.86	0.10	100.28	0.58	0.71
IV	massive	0.07	0.18	14.59	18.92	3.24	9.84	0.45	52.46	0.11	99.86	0.65	0.71
V	massive	0.05	0.26	16.72	25.95	4.92	5.64	0.48	46.52	0.08	100.62	0.82	0.65

Massive >30 vol.% chromite; stratified 15–30 vol.% banded chromite; disseminated <15 vol.% chromite; accessory <5 vol.% chromite. $\#Fe^{2+}$ $Fe^{2+}/(Fe^{2+} + Mg)$, $\#Cr$ $Cr/(Cr + Al)$

data indicate that chromite compositions from layers I and II in the mines of Pedrinhas, Limoeiro and Mato Limpo are characterized by higher Cr and Mg, and low Ti and Fe^{3+}, compared to the corresponding layers in the Cascabulhos

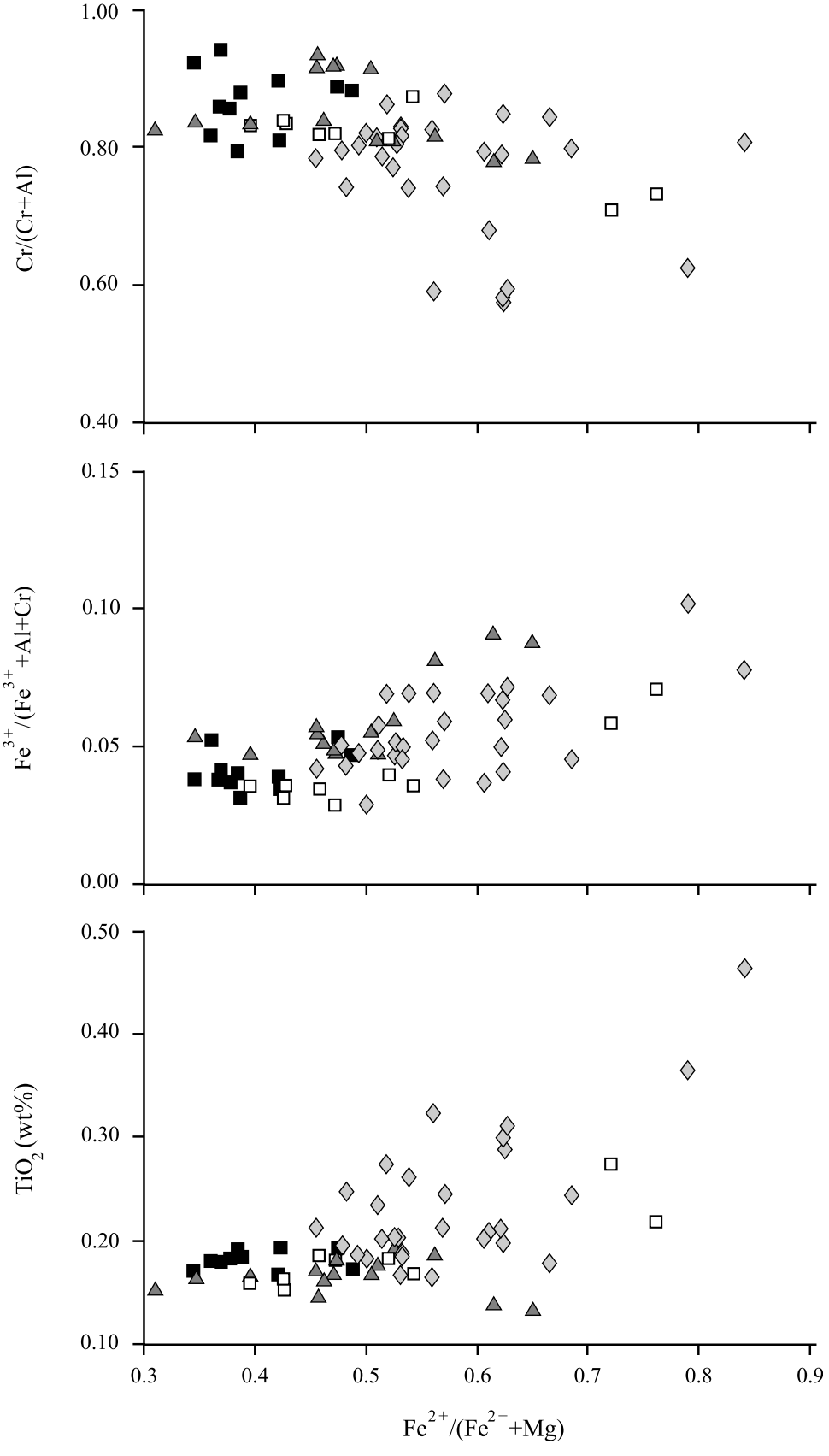
1.00
0.80
0.60
0.40
Cr/(Cr+Al)
0.15
0.10
0.05
0.00
Fe3+/(Fe3+ +Al+Cr)
0.50
0.40
0.30
0.20
0.10
TiO2 (wt%)
0.3
0.4
0.5
0.6
0.7
0.8
0.9
Fe2+/(Fe2+ +Mg)

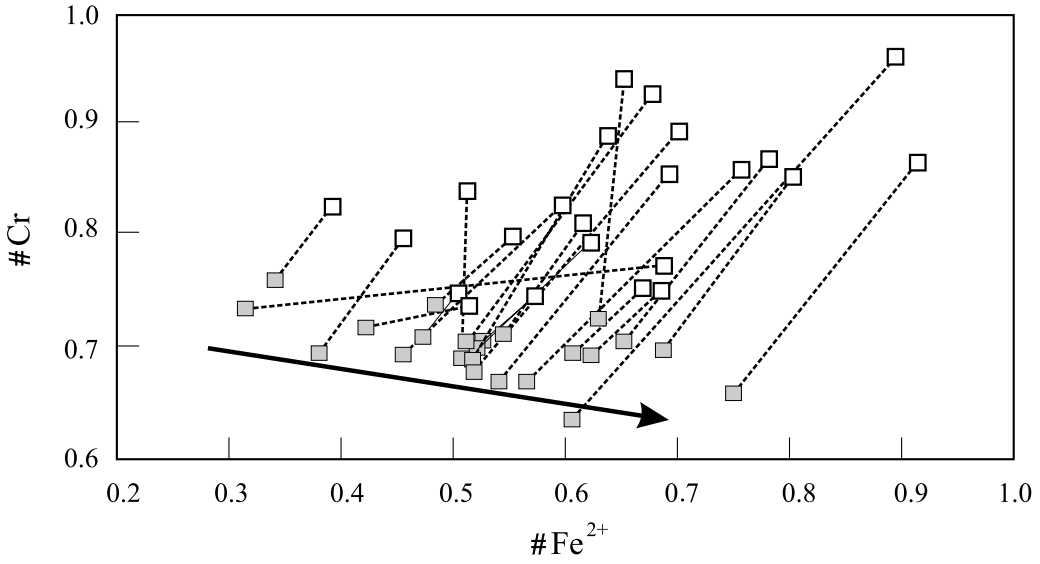

Fig. 4. Compositional zoning of partially altered chromite grains from various chromitite layers of Campo Formoso. Decrease of $\#Cr = Cr/(Cr + Al)$ with $\#Fe^{2+} = Fe^{2+}/(Fe^{2+} + Mg)$ in the unaltered cores (gray square) reflects the igneous fractionation trend (black arrow). The ferrian chromite rims (open square) show combined increase of the #Cr and $\#Fe^{2+}$ ratios as a result of depletion of Al and Mg due to alteration

section. Hence, they extend the covariation trends towards more primitive compositions than those reported by *Lord* et al. (2004). This could arise doubts regarding the stratigraphic correlation of the different cross sections (*de Deus* et al., 1982). Alternatively, it possibly suggests that there were compositional variations of chromite along strike within single chromitite layers, over distances in the order of some kilometers.

The ferrian chromite formed in the first stage of alteration is characterized by a general decrease of Mg, and Al and an increase of Fe^{2+} and Fe^{3+}; thereby compositions are systematically shifted toward higher Cr and Fe^{2+} numbers (Fig. 4). The spongy, late-generation ferrian chromite is not homogeneous, but consists of two intimately intermixed spinel phases characterized by different reflectivity and composition (Fig. 5). The higher reflective phase is compositionally identical to the non-porous ferrian chromite which is in direct contact with the unaltered core. On the contrary, the lower reflective phase has higher Cr with markedly lower total FeO and oxidation ratio $Fe^{3+}/(Fe^{3+} + Fe^{2+})$ (Table 2). Textural relations indicate that the reduced spinel phase, with low oxidation ratio is formed at the expenses of the more oxidized one.

Fig. 3. Compositional variations of major element parameters in unaltered cores of chromite grains reflecting igneous differentiation through stratigraphy (see text for explanation). Note that data from Pedrinhas (black square), Limoeiro (triangle) and Mato Limpo (open square) are characterized by higher Cr and Mg, and low Ti and Fe^{3+}, compared to the corresponding layers in Cascabulhos (diamond). Data from electron microprobe analysis

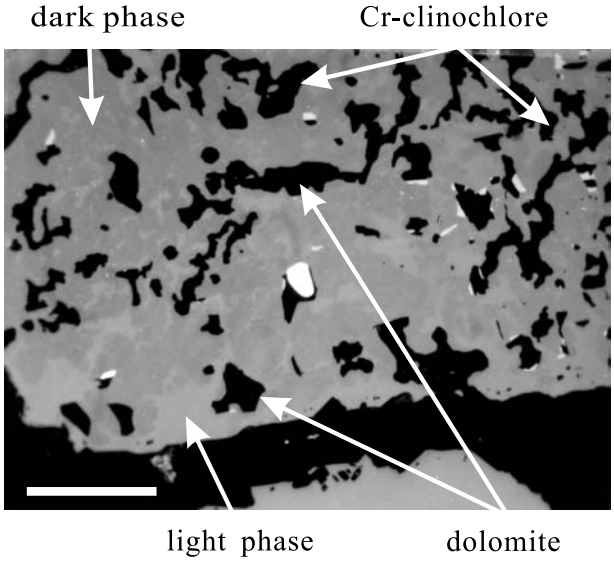

Fig. 5. Reflected light image of the two spinel phases constituting the spongy ferrian chromite of late generation. Pores are filled with chromian clinochlore and dolomite. Minute crystals of millerite and one large grain of laurite are visible; light grey = high $Cr + Fe^{3+}$ ferrian chromite, middle grey = low $Cr + Fe^{3+}$ ferrian chromite, dark = silicate-carbonate matrix. Scale bar = 50 μm

Table 2. *Compositional zoning across the partially altered grain in Fig. 5*

	SiO_2	TiO_2	Al_2O_3	FeO	Fe_2O_3	MnO	MgO	Cr_2O_3	NiO	FeO_{tot}	#Cr	#Mg	#OX
unaltered core													
core 1	0.00	0.25	15.5	22.5	8.32	0.61	7.32	45.5	0.00	30.0	0.66	0.37	0.25
core 2	0.00	0.20	16.2	22.0	7.90	0.55	7.75	45.4	0.00	29.1	0.65	0.39	0.24
core 3	0.00	0.20	16.3	22.1	7.86	0.55	7.70	45.3	0.00	29.2	0.65	0.38	0.24
core 4	0.00	0.23	16.0	22.4	7.71	0.62	7.46	45.5	0.09	29.3	0.66	0.37	0.24
core 5	0.00	0.21	15.2	22.2	8.45	0.64	7.47	45.7	0.13	29.8	0.67	0.38	0.26
solid ferrian-chromite													
Fe-chr 1	0.00	0.28	5.26	26.4	22.2	0.72	3.50	41.6	0.00	46.4	0.84	0.19	0.43
Fe-chr 2	0.00	0.13	12.4	23.6	13.1	0.69	6.20	43.8	0.10	35.4	0.70	0.32	0.33
Fe-chr 3	0.00	0.44	3.70	27.1	24.1	0.65	2.85	41.0	0.18	48.8	0.88	0.16	0.44
light spongy ferrian-chromite													
spongy 1	0.00	0.38	2.10	28.4	24.0	0.80	1.71	42.4	0.20	50.0	0.93	0.10	0.43
spongy 2	0.14	0.47	2.19	27.6	25.9	0.76	2.27	40.7	0.00	50.9	0.93	0.13	0.46
spongy 3	0.10	0.75	1.28	28.3	25.3	0.81	1.6	41.7	0.12	51.1	0.96	0.09	0.46
spongy 4	0.00	0.42	1.36	28.6	25.1	0.78	1.54	42.0	0.14	51.2	0.95	0.09	0.44
dark spongy ferrian-chromite													
spongy 5	0.00	0.40	3.93	28.1	11.8	0.78	2.28	52.7	0.00	38.7	0.90	0.13	0.27
spongy 6	0.00	0.49	3.89	27.3	13.3	0.85	2.69	51.4	0.09	39.3	0.90	0.15	0.30
spongy 7	0.00	0.50	2.28	28.2	15.5	0.86	1.95	50.6	0.11	42.1	0.94	0.11	0.33
spongy 8	0.00	0.52	1.91	28.2	17.2	0.96	1.82	49.4	0.12	43.6	0.95	0.10	0.35
spongy 9	0.09	0.53	2.34	28.4	15.2	0.84	1.76	50.7	0.15	42.1	0.94	0.10	0.32
spongy 10	0.00	0.49	2.32	28.4	15.5	0.77	1.88	50.6	0.00	42.4	0.94	0.11	0.33
spongy 11	0.00	0.57	2.14	28.1	13.9	0.89	1.96	52.4	0.16	40.5	0.94	0.11	0.31

#Cr $Cr/(Cr + Al)$, *#Mg* $Mg/(Mg + Fe^{2+})$, *#OX* $Fe^{3+}/(Fe^{3+} + Fe^{2+})$

Accessory ore minerals

Up to 150–300 ppm total S are present as accessory sulfides, that occur finely disseminated in the chromitites, either as minute blebs (<20 μm) included in fresh chromite or larger aggregates (up to 200 μm) associated with the alteration minerals (ferrian-chromite, chlorite, carbonates). The chromite-included sulfides constitute a negligible proportion of the total sulfide phase present in the chromitites. They consist of Ni–Fe–Cu assemblages, mainly pentlandite with minor chalcopyrite, millerite, bornite, and rare pyrrhotite. In contrast, the sulfides and related phases located in the alteration matrix consist of pentlandite, heazlewoodite, millerite, polydymite, violarite with minor pyrite, unknown Ni–Co sulfarsenides, galena, bismuthinite, Pb-antimonides and native Sb (*Zaccarini* et al., 2005a).

The Ni-sulfides form laths, specks, polygonal or irregular particles located along the cleavage planes of chlorite, sometimes in contact with or included in ferrian chromite. Electron microprobe analyses (Table 3) indicate that heazlewoodite, millerite and polydymite may contain between 0.15 and 12.82 wt% Fe. Pentlandite and polydymite have Co concentrations up to 4.51 wt%. The Cr

Table 3. *Selected electron microprobe analyses of Ni-sulfides from the Campo Formoso chromitites*

	Ni	Cu	Fe	Co	S	As	Cr	Tot
Heazlewoodite Ni_3S_2								
CB1-3	71.40		0.15		26.78	0.06		98.39
CB2-7	71.09		0.51		26.57			98.17
CB3-11	70.04		0.66		26.50	0.05		97.25
LM78-4	69.49		1.82	0.23	27.34			98.88
Pentlandite $(Ni,Fe)_9S_8$								
CB27-2	38.75		25.16	2.18	32.69			98.78
CB27-8	37.35		28.07	1.88	32.44			99.74
CB28-4	37.16		25.74	1.76	32.93			97.59
ML90-13	36.18		25.40	4.33	33.50			99.41
ML90-2	36.63		24.44	4.22	32.72			98.01
PE62-10	45.86		20.35		33.38			99.59
Millerite NiS								
CB21-2	63.15		0.26		35.98	0.24		99.63
ML32-4	57.23		6.78		34.99			99.00
ML35-3	63.21		0.31		35.31			98.83
ML37-1	62.02		3.04		34.59			99.65
Pyrite FeS_2								
LM78-4	0.04	0.71	46.60		51.64			98.99
ML35-2	3.02		42.86		53.37	0.08		99.33
Polydymite Ni_3S_4								
LM74-1	45.04	0.98	3.26	4.51	38.54	0.12	2.57	95.02
ML90-24	37.89	0.41	12.82	2.92	40.94	0.36	0.29	95.63

CB Cascabulhos, *LM* Limoeiro, *ML* Mato Limpo, *PE* Pedrinhas

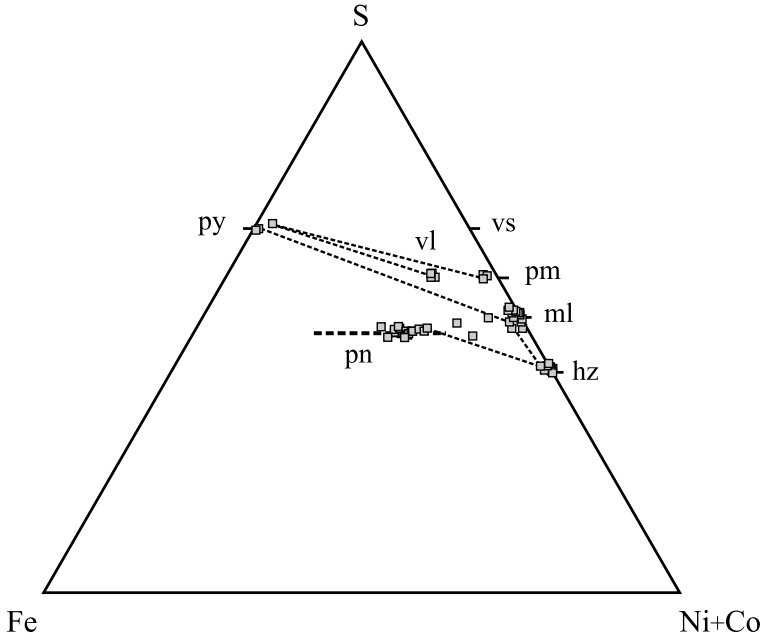

Fig. 6. Phase relations in the Fe-(Ni + Co)-S system for secondary Ni-sulfides disseminated in the intergranular chlorite matrix and carbonate veins of the chromitites of Campo Formoso. Ideal compositions are reported for comparison: *py* pyrite FeS_2, *pn* pentlandite $(Ni,Fe)_9S_8$, *vs* vaesite, NiS_2, *pm* polydymite Ni_3S_4, *vl* violarite $(Ni,Fe)_3S_4$, *ml* millerite NiS, *hz* heazlewoodite Ni_3S_2

detected in polydymite (2.57 wt% Cr) is possibly ascribed to contamination from adjacent chromite. Phase relations in the Fe-(Ni + Co)-S ternary system indicate the existence of two main associations (Fig. 6), related to different stages of alteration. One, containing pentlandite and heazlewoodite as major phases, is found in the chlorite alteration assemblage, whereas the other, consisting of millerite-pyrite, pyrite-polydymite-violarite is predominantly found in the carbonate alteration, along veins or within porous ferrian-chromite rims. Internal textures of composite grains indicate that heazlewoodite replaces pentlandite and may be replaced in turn by millerite. The unknown Ni–Co sulfarsenides occur exclusively as exsolution lamellae in heazlewoodite. Furthermore, the following composite aggregates with Pb, Sb, and Bi were observed: pentlandite-galena, pentlandite-bismuthinite, pentlandite-Pb-antimonide, millerite-pyrite-galena.

Platinum-group element mineralization

PGE distribution

Total PGE concentrations are low (190–464 ppb) in chromitite layers I–V, but increase up to 589 and 918 ppb, respectively in the highest chromitite layers at Cascabulhos (VII) and Limoeiro (VI) (Table 4). At all localities, samples from layers I–V have PGE distributions with Ru > (Os + Ir) > (Rh + Pt + Pd), resulting in a negative slope of the chondrite-normalized patterns, with a distinct positive

Table 4. *PGE concentrations (ppb) in 20 chromitite samples from Campo Formoso*

Locality/layer	Ore-type*	Os	Ir	Ru	Rh	Pt	Pd
Cascabulhos							
I§	massive	51	68	241	9.2	8.3	10
II base	massive	44	70	230	19	8	14
II centre	massive	<26	50	200	16	6	16
II top	massive	<26	33	210	16	<9	<9
III base	massive	<26	18	190	11	<9	11
III top	massive	<26	18	160	14	<9	11
IV base	massive	<26	17	170	18	<9	12
IV centre 1	layered	<26	16	230	15	16	13
IV centre 2	massive	<26	22	250	16	<9	<9
IV top	massive	<26	16	170	15	<9	13
V centre§	massive	28	32	189	19	10	17
VI base	massive	<26	16	160	16	<9	10
VI centre	massive	<26	15	180	17	<9	16
VII	massive	30	60	460	110	200	58
VII§	massive	48	78	391	121	189	72
Pedrinhas							
I§	layered	44	71	283	12	7.1	7.8
I§	massive	23	77	322	12	10	6.9
II§	massive	52	68	310	18	6.8	8.7
III§	massive	51	75	292	19	8.3	8.6
IV	layered	<26	41	220	26	<9	13
IV§	layered	29	43	286	31	12	13
Limoeiro							
I base§	massive	51	78	243	11	7.8	5.9
I centre§	massive	48	56	199	12	8.7	8.8
IV base§	massive	16	32	198	22	12	12
V centre§	disseminated	14	15	132	10	11	7.9
VI centre	massive	<26	30	480	40	30	14
VI top	massive	31	25	480	29	15	<9
Mato Limpo							
I centre§	massive	55	74	268	12	8.6	7.8
I top§	stratified	21	16	211	11	8.1	12
III base§	massive	39	49	182	11	9.5	9.3
V centre§	massive	33	18	199	12	7.9	14
V top§	massive	46	21	248	32	18	21

* See Table 1. §Analysis performed at Modena and Granada

peak of Ru and a chondritic Pt/Pd ratio below unity (Fig. 7). Distributions with $Ru > (Rh + Pt + Pd) > (Os + Ir)$ are encountered in layer VII of Cascabulhos and layer VI of Limoeiro, where the Pt/Pd ratios increase up to 0.89 and 1.84, respectively. As noted by *Lord* et al. (2004), there is a covariation of PGE ratios with chromite composition across the sequence of chromitite layers well exemplified by the weak positive correlation of $\#Fe^{2+}$ in chromite and the bulk-rock Pd/Ir ratio (Fig. 8).

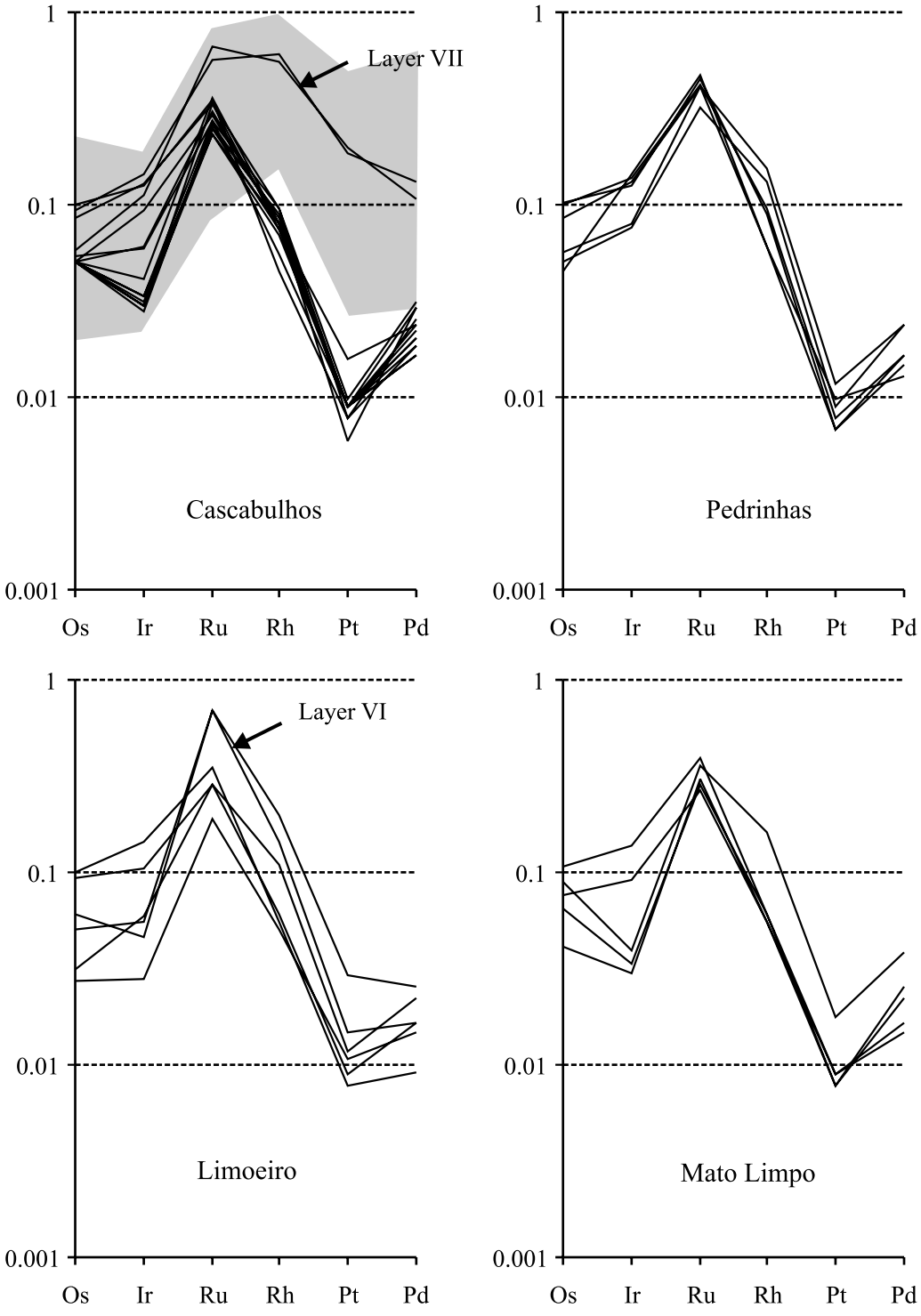

Fig. 7. Chondrite (*Naldrett* and *Duke*, 1980) normalized PGE patterns of the Campo Formoso chromitites. Profiles of layers VII of Cascabulhos and VI of Limoeiro are indicated. The field of chromitites hosted in olivine-orthopyroxene cumulates from the Lower Group of Bushveld (data from *Cawthorn*, 1999) and the upper chromitite layers (C–K) of Stillwater (data from *Page* et al., 1985; *Zientek* et al., 2002) is reported for comparison (gray shaded area)

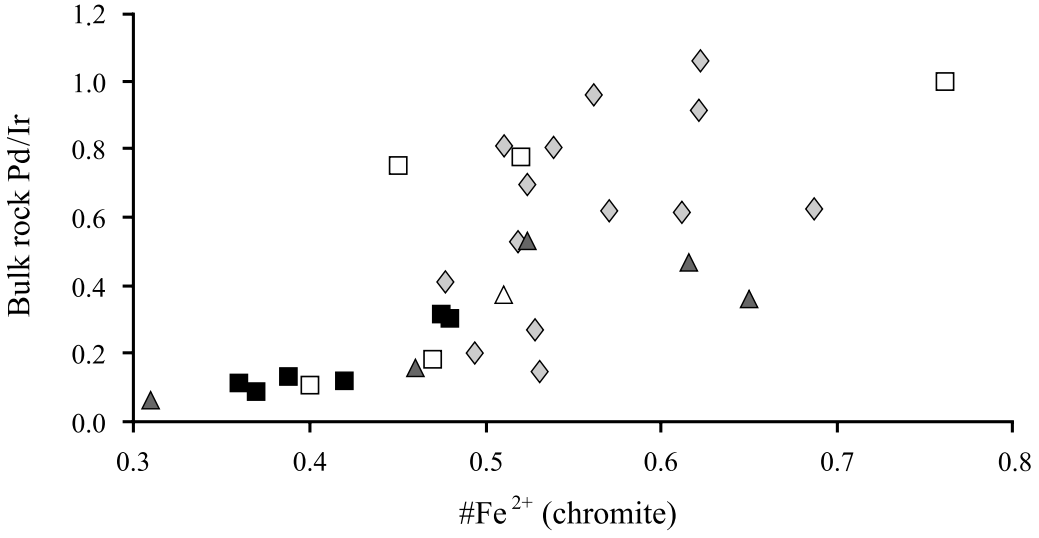

Fig. 8. Positive correlation between the $\#Fe^{2+} = Fe^{2+}/(Fe^{2+} + Mg)$ of chromite and the bulk rock Pd/Ir ratio across the sequence of chromitite layers of Campo Formoso. See text for explanation. Symbols as in Fig. 3

The platinum-group minerals

About two hundred PGM grains, typically less than 10 µm in size and rarely exceeding 20 µm, were discovered in the 66 chromitite samples examined. They are Os–Ir–Ru alloys (osmium) and sulfides (laurite, erlichmanite), Ir–Ru–Rh

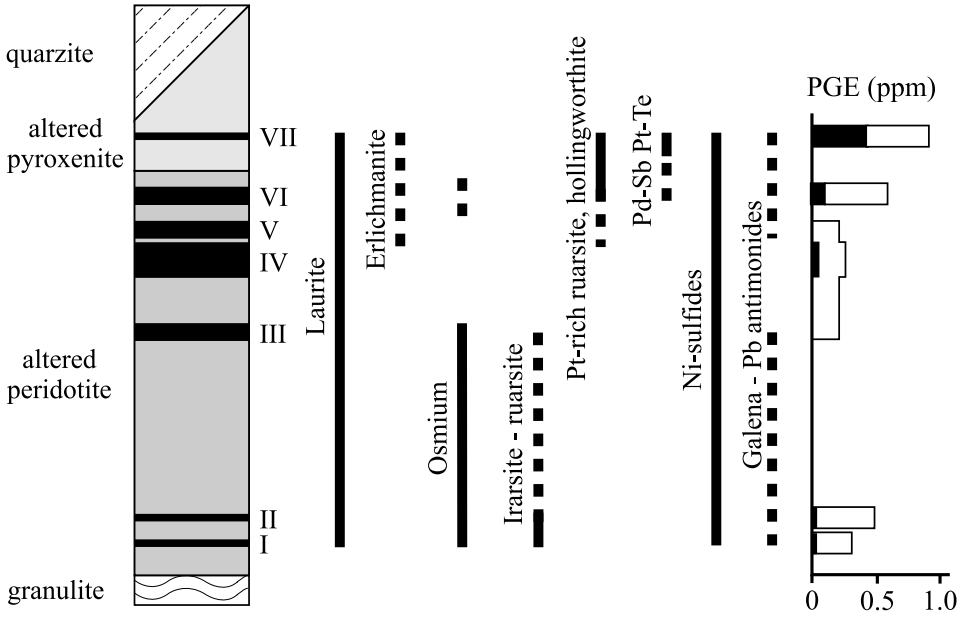

Fig. 9. Distribution of the PGM and accessory ore minerals (Ni-sulfides, galena and Pb-antimonides) across the sequence of chromitite layers. The column to right end shows the total PGE contents (ppm) and relative proportion of IPGE (white) versus PPGE (black)

sulfarsenides (irarsite, ruarsite, hollingworthite), Pd-antimonides (sudburyite, unknown Pd_4Sb_3, unknown Pd(Sb,Bi) and undetermined Pd–Sb). No specific phase of Pt was observed except for undetermined Pt–Te; however, Pt is present as an important constituent of Ru–Rh sulfarsenides (see below). Distribution of the PGM and accessory ore minerals, as well as total PGE contents and relative proportion of IPGE versus PPGE across stratigraphy is presented in Fig. 9. Consistent with geochemical data, Ru-phases are predominant in all layers, whereas Pt–Pd-bearing minerals appear only in layers VI and VII. The accessory Ni-sulfides are ubiquitous, whereas native Sb, Pb-antimonides, galena and bismuthinite have been found sporadically in layers I–III of Pedrinhas, in layers I–III of Limoeiro, in layers I and II of Mato Limpo, and in layers V, VI and VII of Cascabulhos.

Morphology and textural position of the PGM with respect to chromite and the silicate matrix are summarized in Table 5.

Laurite occurs in three different textural positions; i.e. included in the unaltered core of chromite grains (laurite 1), within ferrian-chromite rims and spots (laurite 2), or disseminated in the slicate matrix of chromitite (laurite 3) (Figs. 10 and 11).

Table 5. *Texture and paragenetic association of platinum-group minerals from the Campo Formoso chromitites*

Mineral	Type-composition	Habit	Mineral in contact	Max. size*	No. of grains**
1) PGM included in unaltered core of chromite					
Laurite 1	$(Ru,Os,Ir)S_2$	euhedral	single-phase, pentlandite, Cu-sulfide, rutile	20	48
Osmium	(Os,Ir,Ru)	euhedral	single-phase, chlorite	10	15
Erlichmanite 1	$(Os,Ru,Ir)S_2$	euhedral	laurite	5	1
2) PGM situated in ferrian-chromite rims					
Laurite 2	$(Ru,Os,Ir)S_2$	subeuhedral	chlorite	30	23
3) PGM situated in the silicate-carbonate matrix					
Laurite 3	$(Ru,Os)\ (S,As)_2$	anhedral	single-phase,erlichmanite, irarsite, heazlewoodite, millerite, un. Pb–Sb	45	36
Erlichmanite 2	OsS_2	anhedral	laurite 3, millerite, heazlewoodite	20	4
Irarsite	(Ir,Rh)AsS	anhedral	single-phase	10	6
		exsolved blebs in:	laurite 3, heazlewoodite, millerite	2	several
Hollingworthite	(Rh,Pt,Ir)AsS	anhedral	single-phase, heazlewoodite	15	6
Ruarsite	(Ru,Pt,Rh)AsS	anhedral	single-phase, laurite 3	15	8
Sudburyite	PdSb	anhedral	single-phase	15	1
unk. Pd–Sb 1	Pd_4Sb_3	anhedral	single-phase, bismuthinite	10	5
unk. Pd–Sb–Bi	Pd(Sb,Bi)	anhedral	pentlandite, galena, un. Pb–Sb	5	1
un. Pd–Sb	?	anhedral	pentlandite, galena, un. Pb–Sb	5	12
un. Pt–Te	?	anhedral	heazlewoodite	3	1

* Microns; ** includes minerals identified only qualitatively; *unk.* unknown; *un.* undetermined

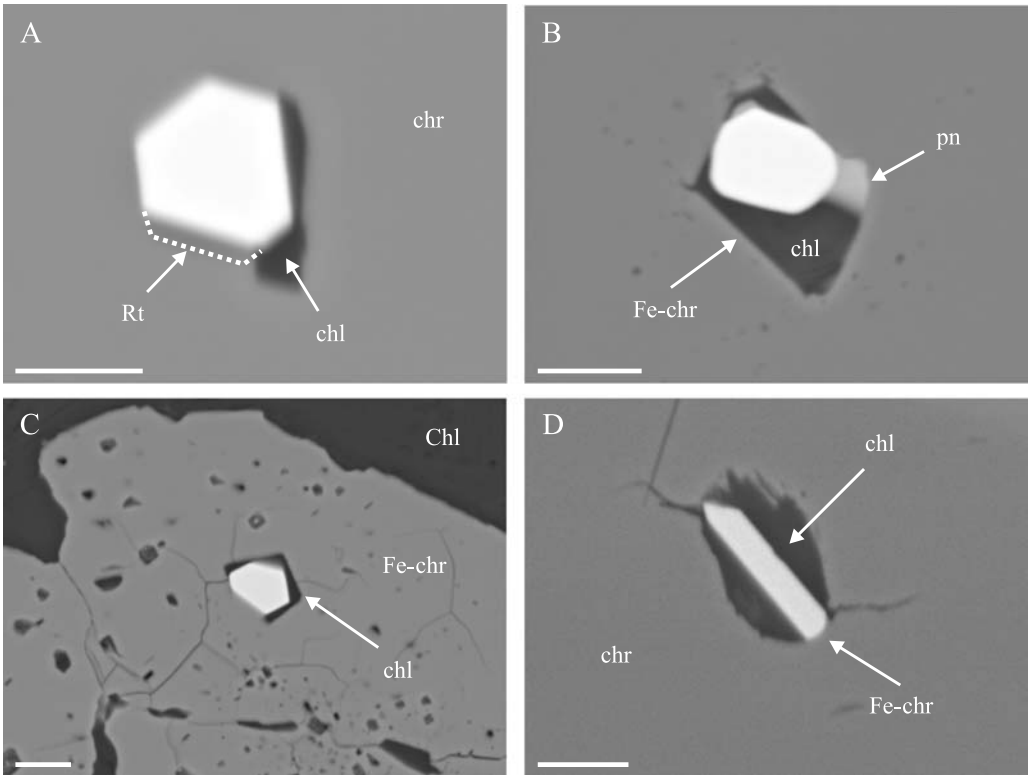

Fig. 10. BSE images of laurite of types 1 and 2. **A** Laurite 1 associated with chlorite and rutile. **B** Laurite 2 associated with chlorite + pentlandite + chlorite in partially altered chromite. **C** Laurite 2 associated with chlorite included in ferrian chromite. **D** Laurite 2 surrounded by chlorite and ferrian chromite, all surrounded by fresh chromite. All laurites have similar compositions (see text for explanation). *chl* Chromian clinochlore, *chr* Unaltered chromite, *Fe-chr* ferrian chromite, *Rt* rutile, *pn* pentlandite. Scale bar = 10 μm

Laurite 1 and 2 are characterized by euhedral to subeuhedral morpholgy and occasionally are associated with rutile and/or pentlandite. In some cases, small chlorite lamellae are part of the inclusions. Their compositions, deduced from electron microprobe analysis (Table 6), define a trend of sympathetic increase in Os and Ir in the Ru–Os–Ir ternary diagram, consistent with the compositional fields of laurite from the stratiform chromitites of Bushveld and Stillwater (Fig. 12). In contrast, laurite 3 has anhedral shape and frequently forms composite grains with Ir–Ru sulfarsenides and Ni–Fe sulfides (pentlandite, heazlewoodite, and millerite). Internal textures suggest that laurite 3 replaces, overgrows, or exsolves from heazlewoodite, millerite, pentlandite and in turn may contain spot-sized exsolutions of irarsite and Ni-sulfides (Fig. 11). The electron microprobe composition of laurite 3 differs from that of types 1 and 2; it has lower Ir content and significant, although scattered, enrichment in Rh, Ni, Fe and As. With a few exceptions, compositions of laurite 3 define a distinctive trend of Ru–Os substitution at low iridium content that extends into the field of erlichmanite (Fig. 12).

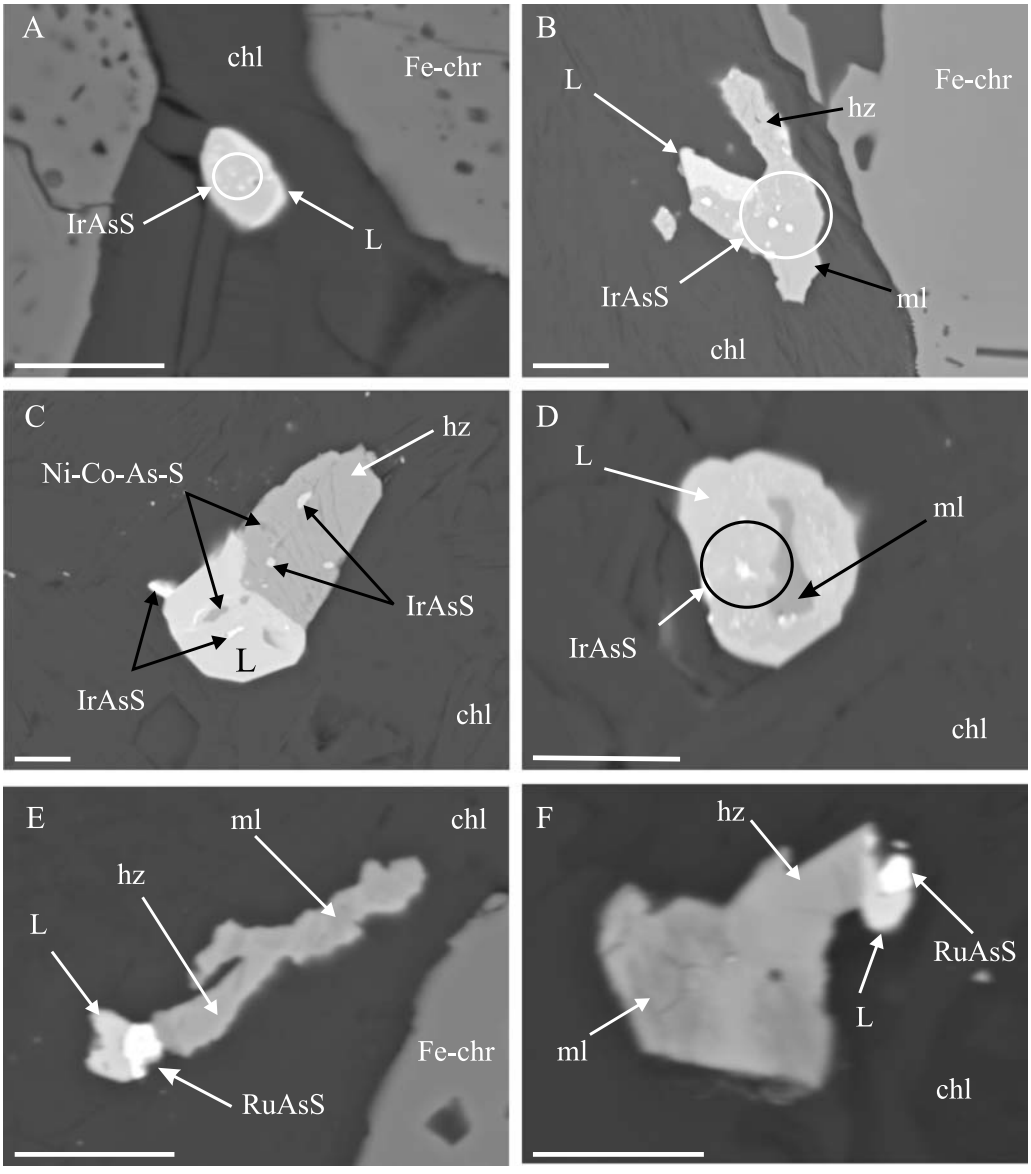

Fig. 11. BSE images of laurite of type 3 occurring disseminated in the Cr-clinochlore matrix of the chromitites. **A** Laurite with irregular inclusions (exsolutions?) of irarsite. **B** Laurite associated with a large grain of heazlewoodite and millerite exsolving (?) irarsite blebs. **C** Laurite associated with heazlewoodite, both containing exsolutions (?) of irarsite and an undetermined sulfarsenide (Ni–Co–A–S). **D** Laurite replacing millerite; irarsite exolutions are visible inside laurite. **E** and **F** Composite grains of laurite and rurasite attached to heazlewoodite-millerite. *hz* Hezlewoodite, *ml* millerite, *L* laurite, *IrAsS* irarsite, *RuAsS* ruarsite; other abbreviations as in Fig. 10. Scale bar = 10 μm

Erlichmanite has been found only in layers V–VII, occurring as either polygonal crystals included in the fresh core of chromite grains (erlichmanite 1), or minute irregular particles attached to laurite 3 and millerite (erlichmanite 2). The

Table 6. *Selected electron-microprobe compositions of laurite from Campo Formoso chromitites*

	Os	Ir	Ru	Rh	Ni	Fe	Cu	S	As	Tot
Laurite 1: euhedral crystals included in unaltered chromite cores										
CB1-2	9.64	6.31	44.70	0.34	0.11	1.73	0.13	37.00	0.00	99.96
CB3-8	8.51	4.97	48.10	0.00	0.14	0.80	0.12	36.80	0.04	99.48
CB28-14	8.49	4.24	48.10	1.22	0.06	1.22	0.00	36.70	0.00	100.03
LM64-9	2.84	1.87	53.00	1.96	0.14	0.90	0.00	37.90	0.00	98.61
LM65-7a	3.44	3.19	53.80	0.00	0.00	0.99	0.00	38.50	0.00	99.92
LM72-1	7.02	0.23	51.20	2.85	0.24	0.58	0.00	37.80	0.00	99.92
LM80-1a	6.44	6.14	49.80	0.39	0.08	0.43	0.00	37.00	0.00	100.28
LM80-4a	6.46	5.82	48.90	0.69	0.08	0.74	0.00	37.00	0.00	99.69
LM82-1	4.99	2.46	51.60	1.76	0.12	0.98	0.00	37.60	0.00	99.51
ML32-3	6.64	5.80	47.30	0.66	0.00	0.72	0.00	36.40	0.00	97.52
ML35-1	4.32	4.81	51.90	0.43	0.08	0.61	0.00	37.20	0.00	99.35
ML90-6	3.46	3.07	53.50	0.00	0.00	1.18	0.00	36.20	0.00	97.41
ML90-7	3.57	3.35	52.40	0.00	0.00	1.42	0.00	36.50	0.00	97.24
ML90-13c	3.19	3.19	54.50	0.00	0.00	0.82	0.00	37.50	0.00	99.20
ML90-15	3.42	3.19	55.30	0.00	0.08	1.22	0.00	37.40	0.00	100.61
ML90-17	3.57	3.00	54.00	0.00	0.00	1.07	0.00	37.40	0.00	99.04
ML90-19	4.18	2.42	52.80	0.62	0.18	1.28	0.06	38.20	0.00	99.74
ML90-21a	3.56	2.69	53.00	0.00	0.00	1.11	0.00	36.90	0.00	97.26
ML90-23	3.03	3.27	55.00	0.25	0.00	0.91	0.06	38.10	0.00	100.62
PE55-1a	5.13	5.51	50.00	0.83	0.00	0.32	0.00	36.50	0.00	98.29
PE59-2a	3.67	4.97	50.10	0.87	0.41	1.67	0.00	38.20	0.00	99.89
PE62-10d	10.42	5.75	43.00	1.50	0.38	0.72	0.11	36.60	0.00	98.48
Laurite 2: euhedral-subeuhedral crystals in ferrian-chromite rims										
CB9-1	3.27	2.60	54.40	0.99	0.00	1.04	0.00	38.60	0.00	100.90
CB27-9	3.72	3.44	52.90	0.95	0.00	0.98	0.00	38.10	0.00	100.09
LM65-2	3.44	2.52	53.20	0.08	0.07	0.95	0.00	37.80	0.00	98.06
LM65-5a	3.45	2.83	53.80	0.00	0.08	0.84	0.00	36.90	0.00	97.90
LM65-5b	3.54	2.94	55.10	0.00	0.07	0.83	0.00	37.50	0.00	99.98
LM65-6	3.61	2.80	54.50	0.00	0.06	0.41	0.00	37.70	0.00	99.08
LM65-9	2.64	2.76	53.50	0.40	0.00	0.70	0.00	36.70	0.00	96.70
LM65-13	3.18	2.83	53.80	0.36	0.00	0.78	0.00	36.60	0.00	97.55
LM75-3a	7.65	5.03	47.40	1.85	0.08	0.87	0.00	36.20	0.00	99.08
LM77-4	6.56	2.73	52.10	0.60	0.14	0.77	0.00	37.70	0.00	100.60
LM79-3	9.16	6.81	45.70	0.84	0.10	0.89	0.00	36.50	0.00	100.00
Laurite 3: anhedral crystals in the chlorite matrix of chromitites										
CB1-3	7.09	1.58	51.70	0.27	0.64	0.36	0.00	37.20	1.24	100.08
CB2-7	0.96	0.20	58.30	0.00	0.30	0.30	0.00	38.70	1.12	99.88
CB3-2	7.70	2.64	49.10	1.00	0.27	0.00	0.00	36.40	0.71	97.82
CB3-11	7.97	2.18	49.60	0.00	0.21	0.26	0.08	36.40	0.95	97.65
CB10-1a	3.03	0.00	55.60	1.70	0.00	0.49	0.00	38.10	1.04	99.96
CB12-2	3.96	0.94	55.50	0.00	0.00	0.50	0.00	39.10	0.30	100.30
CB15-2a	3.97	1.15	49.80	3.00	0.18	1.16	0.00	37.10	1.17	97.53
CB26-2a	6.57	4.39	49.50	0.00	0.71	0.86	0.10	37.80	0.08	100.01
CB27-4a	1.99	0.97	56.00	0.39	0.27	0.92	0.00	38.10	0.91	99.55

(*continued*)

Table 6 (*continued*)

	Os	Ir	Ru	Rh	Ni	Fe	Cu	S	As	Tot
LM64-3	1.26	0.19	55.80	0.40	0.30	2.23	0.00	39.30	0.48	99.96
LM77-1	5.77	3.13	49.50	2.15	0.39	0.46	0.00	37.60	0.99	99.99
LM77-5	10.35	2.16	46.70	3.63	0.20	0.69	0.00	36.70	0.00	100.43
ML86-4	9.98	1.12	51.80	0.00	0.13	0.63	0.00	37.40	0.00	101.06
PE54-2b	10.04	1.63	46.50	0.77	0.46	0.63	0.00	37.00	0.24	97.27
PE54-7a	5.80	0.89	53.50	1.19	0.09	0.41	0.04	37.70	0.24	99.86
PE59-7	8.48	2.03	48.90	1.05	0.28	0.65	0.09	35.90	0.31	97.69

Sample labels as in Table 3

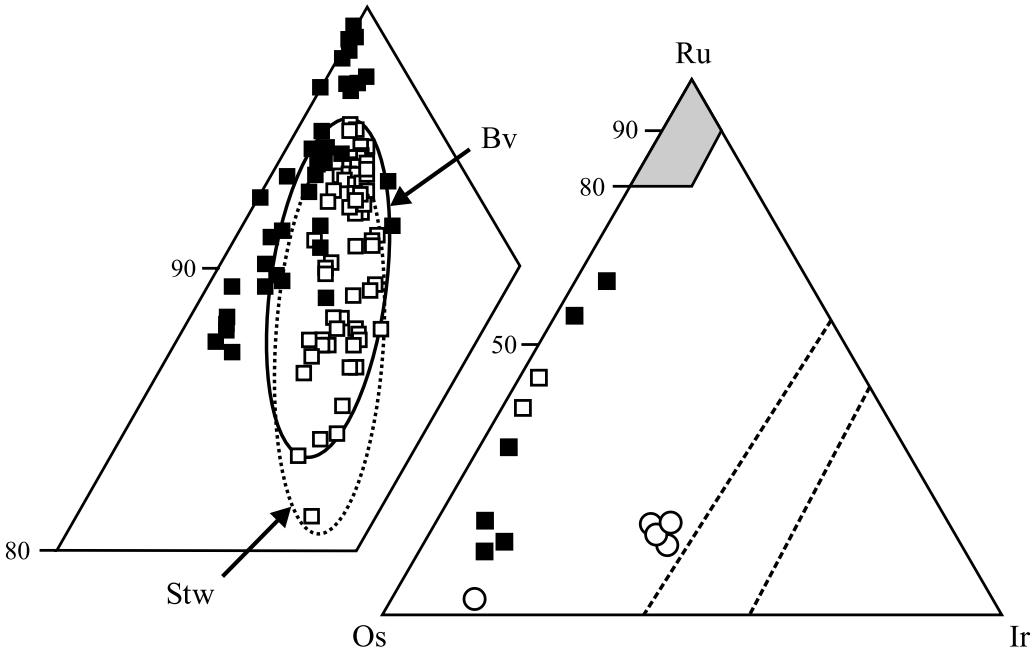

Fig. 12. Compositions of different types of laurite and erlichmanite from the Campo Formoso chromitites projected on the ternary diagram Ru–Os–Ir. Open square = laurite 1 and 2 and erlichmanite 1; black square = laurite 3 and erlichmanite 2; open circles = Os-alloys; Bv = field of laurite inclusions in the Bushveld chromitites (after *Zaccarini* et al., 2002); Stw = field of laurite inclusions in the Stillwater chromitites (after *Cooper* et al., 2005)

two types of erlichmanite have similar compositions in terms of Ru–Os–Ir (Fig. 12) although, erlichmanite 2 shows a consistent enrichment in As (Table 7).

Osmium was encountered exclusively in layers I–III of Pedrinhas, Limoeiro and Mato Limpo, and sporadically in layer VI of Cascabulhos. The mineral occurs as euhedral crystals included in unaltered chromite cores, sometimes in contact with minute lamellae of chlorite, but it was never found within the chlorite matrix. Osmium from layers I–III is rich in Ir and Ru ($Os_{43}Ir_{35}Ru_{14}Fe_8$) in contrast to osmium from layer VI, which has distinctly lower Ir and Ru, and higher Fe ($Os_{70}Ir_{10}Ru_2Fe_{18}$) (Fig. 12, Table 7).

Table 7. *Selected electron microprobe analyses of PGM from Campo Formoso chromitites*

	Os	Ir	Ru	Rh	Pt	Pd	Ni	Cu	Fe	S	As	Sb	Bi	Total
*Osmium**														
LM72-2	47.3	39.6	6.54	0.00	0.00	0.00	0.65	0.00	4.19	0.35	0.00	n.a.	n.a.	98.64
PE54-2a	49.6	38.8	8.25	0.00	0.00	0.00	0.00	0.00	1.90	0.00	0.00	n.a.	n.a.	98.55
PE54-5	49.3	38.6	8.24	0.00	0.00	0.00	0.00	0.37	2.08	0.00	0.00	n.a.	n.a.	98.59
ML86-1	47.4	40.2	9.17	0.00	0.00	0.00	0.00	0.44	1.34	0.00	0.00	n.a.	n.a.	98.55
CB23-1	79.3	12.0	0.94	0.33	0.00	0.00	0.60	0.65	4.75	0.00	0.00	n.a.	n.a.	98.57
Erlichmanite														
CB21-1**	58.4	8.39	4.77	0.12	0.00	0.00	0.35	0.00	0.71	25.2	3.48	n.a.	n.a.	101.42
CB21-2**	54.8	10.1	5.41	0.12	0.00	0.00	0.59	0.19	0.70	24.6	4.20	n.a.	n.a.	100.71
CB26-1*	50.2	3.61	9.61	0.10	0.00	0.00	1.15	0.11	0.73	34.4	0.00	n.a.	n.a.	99.91
*Irarsite***														
CB1-3	0.00	45.3	0.00	14.5	0.00	0.00	2.38	0.50	0.95	12.7	23.6	n.a.	n.a.	99.88
CB2-7	0.55	36.8	1.68	11.6	0.00	0.00	0.00	0.00	0.96	16.0	32.3	n.a.	n.a.	99.89
CB3-11	0.00	54.4	0.00	3.38	0.00	0.00	1.26	0.67	0.68	12.0	27.5	n.a.	n.a.	99.89
CB3-11	0.00	54.7	0.00	3.62	0.00	0.00	1.05	0.62	0.73	13.0	26.2	n.a.	n.a.	99.92
CB15-2a 1	0.18	29.3	1.26	27.0	0.00	0.00	0.25	0.35	0.95	15.5	25.0	n.a.	n.a.	99.79
*Hollingworthite***														
CB15-2a 2	0.23	29.0	0.00	26.6	0.00	0.00	0.28	0.29	1.09	15.7	26.7	n.a.	n.a.	99.89
CB15-2a 3	0.00	28.8	1.23	26.5	0.00	0.00	0.27	0.35	1.08	15.2	26.5	n.a.	n.a.	99.93
*Ruarsite***														
CB27-4b 1	1.12	2.44	15.5	9.43	22.1	0.00	1.89	0.00	0.97	14.0	33.4	n.a.	n.a.	100.85
CB27-4b 2	0.20	2.78	14.3	11.5	20.3	0.00	1.87	0.00	1.57	15.1	32.2	n.a.	n.a.	99.82
CB27-4b 3	0.14	3.00	15.1	10.5	21.2	0.00	1.64	0.00	1.00	13.5	33.8	n.a.	n.a.	99.88
CB27-4c	0.19	2.74	14.1	11.3	20.0	0.00	1.86	0.00	1.55	14.9	31.7	n.a.	n.a.	98.34
CB30-1	0.11	12.37	8.8	9.58	19.6	0.00	0.00	0.00	0.00	14.4	33.0	n.a.	n.a.	97.91
*Pd-antimonides***														
CB28-6a 3	0.00	0.00	0.00	0.00	0.35	50.4	0.75	0.00	0.00	0.00	0.00	45.3	0.22	97.02
CB28-10	0.00	0.00	0.00	0.00	0.78	39.1	1.35	0.00	0.00	0.00	0.00	32.3	24.9	98.43
CB28-11	0.00	0.00	0.00	1.21	0.15	41.3	1.80	0.00	0.00	0.00	0.00	54.8	0.00	99.26

* Included in unaltered chromite cores; ** included in the chlorite matrix; *n.a.* not analyzed, sample labels as in Table 3

Discrete crystals of Ir–Ru–Rh sulfarsenides were found only in the chlorite matrix of the chromitites, either isolated or attached to laurite 3 and Ni-sulfides (Fig. 11). Irarsite is confined to layers I–III, hollingworthite starts to appear from layer V upwards, whereas ruarsite occurs in all layers, although with distinct compositions in relation to stratigraphy (Table 7). Irarsite and ruarsite from layers I to III contain abundant Os, Rh, Ni, Fe and trace amounts of Cu, but no Pt and Pd. Their compositions define a trend of Ir–Ru substitution, indicating solid solution between the two phases (Fig. 13). Ruarsite and hollingworthite in layers V–VII are extremely poor in Os and Ir (Table 7) and both define trends of Pt enrichment from layers V to VII. The Ru–Rh sulfarsenides are the main carriers of Pt in layer VII, containing up to 27.0 and 8.12 wt% Pt, respectively (Table 7).

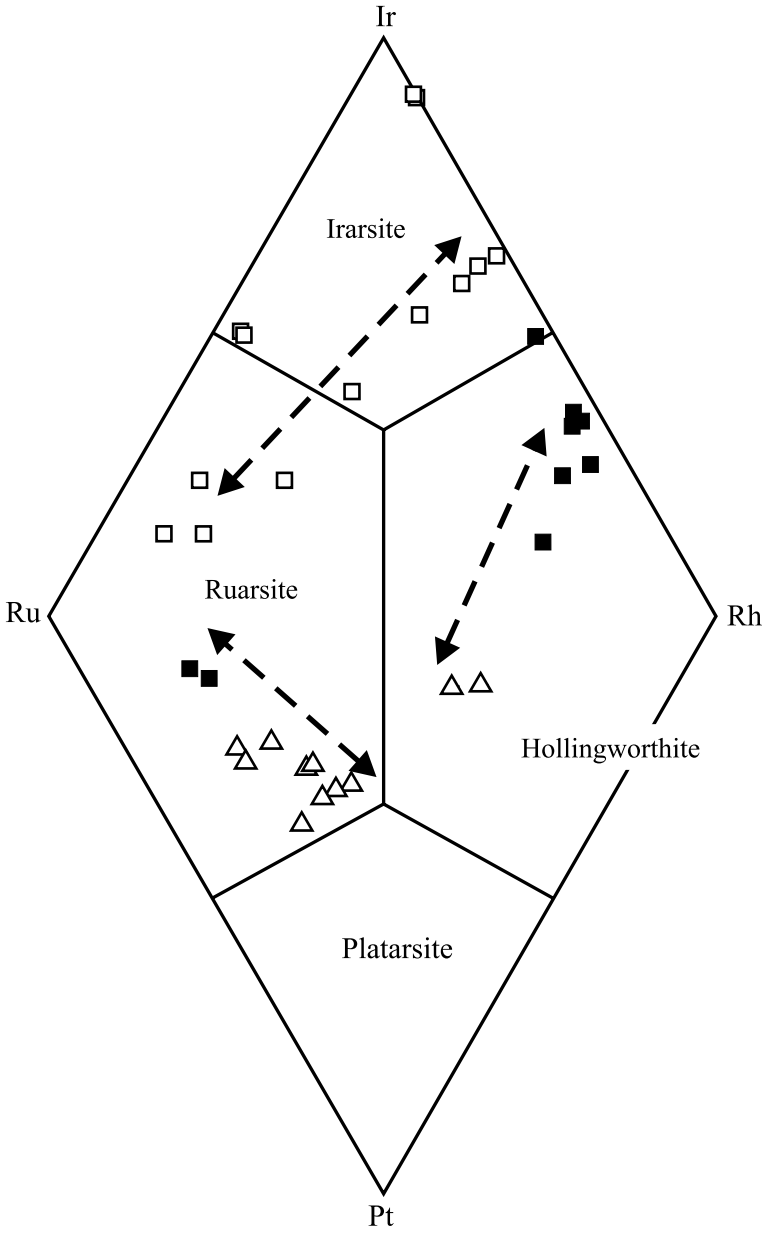

Fig. 13. Compositions of different sulfarsenides from the Campo Formoso chromitites projected on the quaternary diagram Ru–Ir–Rh–Pt. Open square = irarsite and ruarsite from layers I–III; black square = ruarsite and hollingworthite in layers V–VII; open triangles = Pt-rich ruarsite and hollingworthite from layer VII of Cascabulhos. Arrows define possible solution series across the sequence of chromitite layers

The Pd-antimonides were found only in the chlorite matrix, independent of laurite, either as single phases or composite grains with pentlandite and galena (Fig. 14D) or unknown Pb–Sb compounds (*Zaccarini* et al. 2005). Electron microprobe analyses (Table 7) indicate that sudburyite (ideal PdSb) contains minor amounts of Rh (1.21 wt%), Pt (0.15 wt%) and Ni (1.80 wt%), with a recalculated

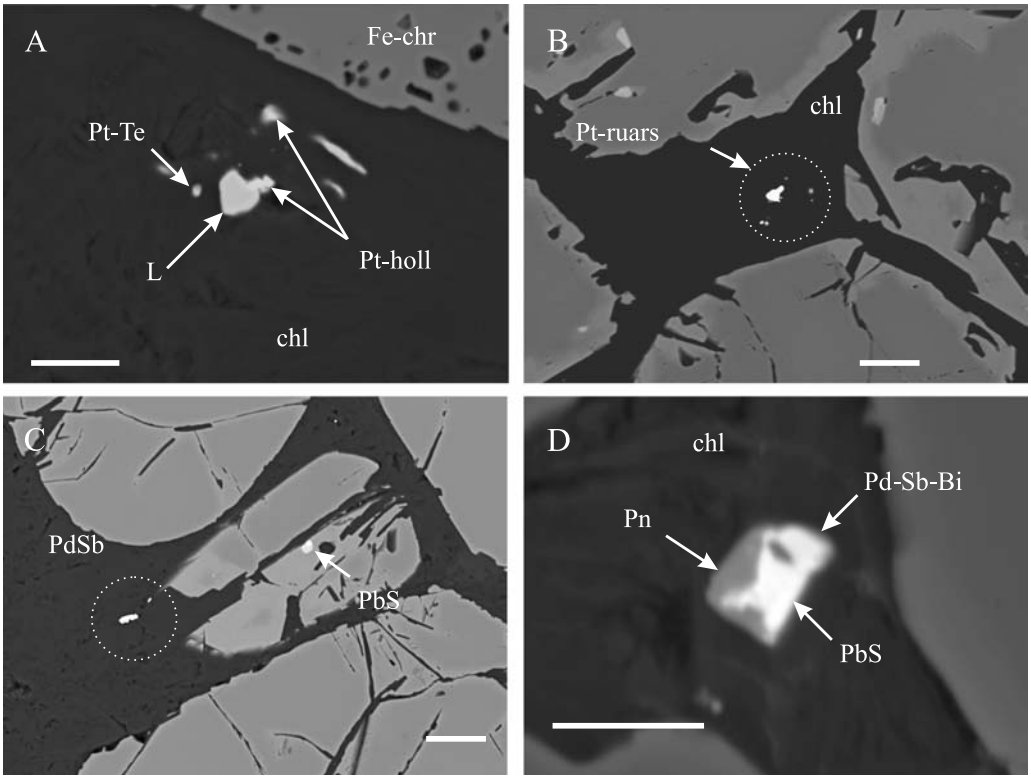

Fig. 14. BSE images of Pt- and Pd-bearing PGM disseminated in the Cr-clinochlore matrix of the chromitite layer VII of Cascabulhos. *Pt–Te* unknown Pt-telluride, *Pt-holl* Pt-rich hollingworthite, *Pt-ruars* Pt-rich ruarsite, *PdSb* sudburyite, *Pd–Sb–Bi* unknown Pd(Sb,Bi), *PbS* galena. Other abbreviations as in Figs. 6 and 10. Scale bar = 10 μm

formula $(Pd_{0.88}Rh_{0.03}Pt_{0.003}Ni_{0.07})_{0.983}Sb_{1.017}$. The unknown Pd(Sb,Bi) phase has the formula $(Pd_{0.94}Pt_{0.01}Ni_{0.06})_{1.01}(Sb_{0.68}\ Bi_{0.31})_{0.99}$. A Pd-antimonide with similar composition has been reported in concentrates from the Driekop mine of the Bushveld complex (*Stumpfl*, 1961; *Tarkian* and *Stumpfl*, 1975). It is mentioned in the list of "unidentified PG-phases" of *Daltry* and *Wilson* (1997) and appears as "unnamed G" and "unnamed mineral 1024" in the compilations of *Cabri* (1972) and the *Nickel* and *Nicholls* MINERALS program, respectively (*Merchel F.*, personal communication). Based on stoichiometry it could be ascribed to a Bi-bearing sudburyite or the Pd-analogue of stumpflite (ideally PtSb). The unknown Pd_4Sb_3 has the formula $(Pd_{3.85}Pt_{0.02}Ni_{0.10})_{3.97}(Sb_{3.02}\ Bi_{0.01})_{3.03}$, and may be similar to "unnamed 493" from Yubdo (*Evstigneeva* et al., 1992) (*Merchel F.*, personal communication).

Discussion

Primary magmatic features of the chromite – PGE mineralization

Repeated cycles of hydrothermal alteration have completely modified the magmatic silicate assemblage of the Campo Formoso chromitites, however, compositional

features of chromite as well as distribution and mineralogy of PGE still display characteristics attributable to igneous fractionation.

The question of whether chromite cores may change their composition in response to formation of the ferrian-chromite rims is debated, because some authors (e.g. *Roeder*, 1994) have warned about possible core-rim metal exchanges during alteration. At Campo Formoso, compositional variations involve a decrease of #Cr and #Mg, accompanied by an increase in total Fe, Fe^{3+} and Ti with increasing distance from the base of the intrusion. This trend is similar to those commonly observed in stratiform chromitites of the Bushveld type (*Stowe*, 1994). In particular, they are consistent with those in successive chromitite sequences hosted in olivine-orthopyroxene cumulates located close to the base of layered intrusions (i.e.: the Lower Critical Zone of the Bushveld complex). These observations infer that, if re-equilibration of the grain cores occurred, it did not substantially modify major element ratios.

In analogy, the pattern of PGE distribution over the sequence of chromitite layers at Cascabulhos reflects fractionation in a magmatic system (*Lord* et al., 2004). Geochemical and mineralogical data presented in this paper are in agreement with this conclusion, showing fractionation of IPGE in layers I–V, at all localities, and relative enrichment of Pt and Pd in layers VI and VII of Cascabulhos and Limoeiro. This trend is very similar to that observed in ultramafic-hosted chromitite layers of the Bushveld-type layered intrusions such as Bushveld, Stillwater and Great Dyke (*Cawthorn*, 1999; *Page* et al., 1985; *Zientek* et al., 2002; *Oberthür*, 2002). Furthermore, the results of the mineralogical study confirm that laurite 1, osmium and erlichmanite 1, which occur as inclusions in the unaltered cores, are magmatic in origin. Compositional similarity of laurite 1 with primary laurites from undisturbed chromitite layers of Bushveld and Stillwater supports this hypothesis. Morphology of these PGM suggests mechanical entrapment by chromite nucleating around them, as it has been demonstrated for several chromitite occurrences (e.g. *Garuti* et al., 1999; *Zaccarini* et al., 2002).

The mineralogy of the primary PGM reflects fractionation in a regime of low sulfur fugacity, e.g. between the stability field of RuS_2 and values slightly exceeding the boundary of the reaction $Os + 2S = OsS_2$, below sulfur saturation. The association of primary PGM with chlorite included in chromite does not reflect equilibrium crystallization. Under appropriate water pressure (5–6 kbar), chlorite can be stable at maximum temperatures in the order of 700–800 °C (*Evans*, 1977) and therefore cannot be part of the high-temperature magmatic assemblage. The mineral probably formed by alteration of primary mafic silicates coexisting with the PGM in composite inclusions. The fact that laurite 2 associated with ferrian chromite rims is compositionally identical to laurite 1 indicates that PGM inclusions have occasionally survived alteration of the chromite host.

Effects attributable to secondary hydrothermal processes

Several lines of evidence support the opinion that the group of PGM now found in the chlorite matrix (laurite 3, erlichmanite 2, Ir–Ru–Rh sulfarsenides, Pd-antimonides) do not represent relict magmatic minerals. Noteworthy are the para-

genetic relationships of the PGM with the Ni-sulfides disseminated in the chlorite matrix indicating co-crystallization and replacement. The mineralogy of the Ni-sulfides is not consistent with equilibration of an immiscible sulfide liquid, neither does it reflect simple in-situ oxidation of intercumulus sulfide droplets. There is no sign that the Ni-sulfides and the PGMs underwent any type of in-situ oxidation. Literature data show that oxidation of magmatic sulfide blebs leads to an assemblage characterized by magnetite + pentlandite, sometimes accompanied by heazlewoodite ± awaruite, essentially within the limits of the original droplet (*Eckstrand*, 1975; *Thompson* et al., 1984). In situ alteration of PGM usually involves desulfidation and oxidation that gives rise to PGE alloys and/or oxides (*Stockman* and *Hlava*, 1984; *Ferrario* and *Garuti*, 1988; *Garuti* and *Zaccarini*, 1997; *Garuti* et al., 1997; *Zaccarini* et al., 2005b) in which relics of the original primary phase may be preserved (*Garuti* et al., 1998; *Zaccarini* et al., 2004). None of these ore mineral assemblages was found in the chromitites of Campo Formoso. The present Ni-sulfide-PGM association appears to be in equilibrium with the chlorite-ferrian chromite assemblage and, therefore, is believed to have formed concomitant with this stage of alteration, after the low-grade regional metamorphism that caused the complete serpentinization of the ultramafic rocks of Campo Formoso.

Since the magmatic distribution pattern of the PGE is still preserved on the hand specimen scale, we conclude that any remobilization probably occurred on a small scale, within the limit of single chromitite layers. This implies that the source material for the formation of the secondary PGM-Ni-sulfide assemblage was probably a PGM-bearing sulfide precursor, originally located in intergranular spaces or at the rim of chromite grains. Its mineralogical nature (sulfide, alloy, oxide) is unknown. We may only suggest that the PGM probably were affected by a first step of alteration during serpentinization, and were then reworked by subsequent hydrothermal events characterized by chlorite-carbonate alteration (*Boukili* et al., 1984).

Conditions for PGE-mobility

Boukili et al. (1983, 1984) tentatively proposed a connection between chloritization of the ultramafic rocks of Campo Formoso and penetrative infiltration of fluids emanating from the nearby granite. The recent discovery of a granite-compatible suite of exotic minerals (monazite, apatite, fluorite, and galena) in the chromitites supports this hypothesis (*Zaccarini* et al., 2005a) and suggests that the metasomatic fluid phase had a calc-alkaline geochemical character similar to solutions in porphyry-copper hydrothermal systems.

The alteration assemblage of the chromitites requires that the initial solution carried H_2O and CO_2 and was moderately to strongly acidic, with relatively high oxygen fugacity (fO_2). Chloritization probably occurred at temperatures between 200 and 400 °C, as deduced from the P_{H_2O} – T °C stability of the alteration mineral assemblage (*Boukili* et al., 1984) and chlorite geothermometry (*Zaccarini* et al., 2005a). A major consequence was the breakdown of magmatic chromite, giving rise to the ferrian chromite rims, and transformation of the assemblage serpentine + chromite into chlorite + ferrian chromite. Ferrian-chromite alteration involves transfer of Cr, Al, and Mg from chromite to chlorite (*Beeson* and *Jackson*, 1969;

Bliss and *MacLean*, 1975; *Boukili* et al., 1984). At the same time water is reduced by extraction of O to oxidize Fe^{2+} (in chromite) to Fe^{3+} (in ferrian-chromite), thereby release of H_2 in the system causes reducing conditions in the surroundings of altered chromite grains. Progressive increase of the CO_2/H_2O activity ratio marks the transition to the ''carbonatization stage''. Ferrian chromite of the first generation becomes unstable and is transformed into a porous aggregate intermixed with dolomite, magnesite and chlorite. The decrease of total FeO in spongy ferrian chromite indicates that Fe is preferentially dissolved with respect to Al, Mg, and Cr, with concomitant change of the oxidation state of iron from Fe^{3+} to Fe^{2+}. This reaction liberates O_2, and drives the redox to oxidizing conditions again. The oxygen fugacity of the solution fluctuated greatly during alteration, decreasing initially from oxidizing to reducing, during oxidation of chromite, and arising again to oxidizing as a result of the carbonatization reactions. The mineralogy of Ni-sulfides in equilibrium with laurite 3 and the other secondary PGM is characterized by relatively low S/Me atomic ratios generally less than or equal to unity (pentlandite, heazlewoodite, millerite), and clearly reflects deposition under reducing conditions. In contrast, sulfides with S/Me higher than unity (pyrite, polydymite, violarite) precipitated when the redox condition became oxidizing, and conspicuously they do not associate with PGM. We suggest that mobilization of the PGE took place during the early oxidation stage, presumably by formation of bisulfide or chloride complexes as dissolved species (*Pan* and *Wood*, 1994; *Xiong* and *Wood*, 2000). Soon after, the PGE were redeposited as sulfides and sulfarsenides at the reducing front around chromite grains. The subsequent stage of carbonatization affects the chromitites along veins and cracks and did not substantially modify the distribution and the mineralogy of the newly formed PGM.

It has been proposed that the hydrothermal fluids emanating from the Campo Formoso granite have introduced incompatible elements in the chromitite alteration system, including such as Pb, Sb and Bi (*Garuti*, 1991; *Zaccarini* et al., 2005a). The PGM display a remarkable enrichment in As, and heazleewoodite occasionally exsolves a Ni–Co sulfarsenide. Whether As was added during hydrothermal alteration or was already part of the magmatic assemblage remains an open question. We note that primary PGM included in chromite are sulfides and alloys and do not contain significant As. If As was carried in the intercumulus PGM precursors, we have to admit an increase of the As/S activity ratio as a result of fractionation at high temperature (e.g.: *Merkle*, 1992; *Rudashevsky* et al., 1992; *Garuti* et al., 1999). Therefore, the secondary Ir–Ru–Rh sulfarsenides now occurring interstitial to chromite, at Campo Formoso, may well represent the product of reworking of primary magmatic As-rich phases. On the other hand, there are natural examples showing that PGM can be metasomatically enriched in As under a range of temperatures including those typical of hydrothermal systems (*Zaccarini* et al., 2002). The fact that there is no evident stratigraphic control in the distribution of sulfarsenides through the sequence of chromitite layers, may indicate that As could migrate over longer distances than the PGE due to its higher mobility, having been redistributed more homogeneously during the hydrothermal alteration. There is, however, no conclusive evidence for a large scale migration of As, therefore the hypothesis that also As was introduced from the granitic fluids via hydrothermal metasomatism cannot be excluded.

Concluding remarks

1) The study of chromitite samples from four sections of the Campo Formoso layered intrusion indicates that hydrothermal metasomatism has not substantially disturbed the chromite – PGE mineralization. Primary composition of chromite is preserved within chromite cores. Furthermore, as previously proposed by *Lord* et al. (2004), the PGE distribution patterns are consistent with magmatic fractionation processes, still displaying overall increase of the PPGE/IPGE ratio through the sequence of chromitite layers upwards.
2) The detailed investigation of the PGM paragenesis, however, indicates that there was a considerable mineralogical reworking of the PGE mineralogy, depending on the textural position of PGM grains with respect to chromite crystals and silicate matrix. Only the PGM located in the unaltered core of chromite grains remained unaltered. In contrast, the PGM located in the Cr-clinochlore matrix of chromitites underwent equilibration under rapidly changing redox conditions in the hydrothermal system.
3) The preferential, if not exclusive, occurrence of Rh, Pd, Pt phases in the silicate matrix of the chromitite layers VI and VII has important implications for the recovery of these metals.
4) The case of Campo Formoso seems to indicate that PGE are mobile in metamorphic hydrothermal systems, but only over small distances. In contrast, their mineral carriers (PGM) appear to be largely unstable and are readily re-equilibrated by dissolution-precipitation mechanisms in response to rapidly changing redox conditions, at temperatures compatible with the common stability field of chlorite, possibly in a range between 200 and 300 °C.

Acknowledgements

Significant improvement of this paper was possible thanks to the comments of two referees: F. Melcher and M. Tarkian, as well as the editorial input of J. G. Raith Many thanks go to the staff of Ferbasa for the hospitality offered to G.G. and access to the mining sites. One of us (F.Z.) is grateful to the Austrian Science Fund (Lise Meitner fellowship no M866 and M738) for the possibility to spend two years at the University of Leoben.

References

Augé T (1985) Platinum-group minerals inclusions in ophiolitic chromitite from the Vourinos Complex, Greece. Can Mineral 23: 163–171

Augé T (1987) Chromite deposits in the northern Oman ophiolite: mineralogical constraints. Mineral Deposita 22: 1–10

Augé T (1988) Platinum-group mineral in the Tiébaghi and Vourinos ophiolitic complex: genetic implications. Can Mineral 26: 177–192

Augé T, Johan Z (1988) Comparative study of chromite deposits from Troodos, Vourinos, North Oman and New Caledonia ophiolites. In: *Bissonnas J, Omenetto P* (eds) Mineral deposits within the European community. Springer, Berlin Heidelberg New York, pp 267–288

Beeson MH, Jackson EJ (1969) Chemical composition of altered chromites from the Stillwater Complex, Montana. Am Mineral 54: 1084–1100

Bliss NW, MacLean WH (1975) The paragenesis of zoned chromite from central Manitoba. Geochim Cosmochim Acta 39: 973–990

Boukili H, Novikoff A, Besnus Y, Soubies F, Queiroz C (1983) Petrologie des produits de l'alteration des roches ultrabasiques à chromites de Campo Formoso. Etat de Bahia – Brésil. Sci Geol Mem 72: 19–28

Boukili H, Novikoff A, França J (1984) Mineralogie et géochimie des chlorites et hydroxycarbonates chromitifères de Campo Formoso, Bahia, Brésil. Cah ORSTOM sér Géol XIV/2: 141–152

Cabri LJ (1972) The mineralogy of the Platinum-group elements. Minerals Sci Engng 4: 3–29

Calas G, Manceau A, Novikoff A, Boukili H (1984) Comportement du chrome dans les minéraux d'altération du gisement de Campo Formoso (Bahia, Brésil). Bull Mineral 107: 755–766

Cawthorn RG (1999) Geological models for platinum-group metal mineralization in the Bushveld complex. S Afr J Sc 95: 490–498

Constantinides CC, Kingston CA, Fisher PC (1980) The occurrence of platinum-group minerals in the chromitites of Kokkinorotsos chrome mine, Cyprus. In: *Panayiotou A* (ed) Ophiolites. Proceedings of the International Ophiolite Symposium (Cyprus 1979), Geological Survey Department Nicosia Cyprus: pp 93–101

Cooper RW, Garuti G, Zaccarini F (2005) Platinum Group Minerals distribution in chromitite layers of the Stillwater complex (Montana, USA). In: *Törmänen TO, Alapieti TT* (eds) Platinum-Group Elements – from genesis to benefication and environmental impact. Platinum 10th International Platinum Symposium, August 8–11, 2005, Oulu Finland. Extended Abstracts: pp 58–61

Daltry VDC, Wilson AH (1997) Review of platinum-group mineralogy: compositions and elemental associations of the PG-minerals and unidentified PGE-phases. Mineral Petrol 60: 185–229

de Deus PB, d'El Rey LJH, Hasui Y, Lima e Silva F, Mandetta P, de Oliveira JG, Franke ND, Carvalho PR, de Moraes JAC, Miola W, Vianna JS, Duarte PM, Qeiroz WA (1982) Caraíba, Pedrinhas and Andorinhas minas, Bahia State: copper and chrome in Archean and/or Proterozoic rocks. Intern. Symposium on Archean and Early Proterozoic geological evolution and metallogenesis, Salvador, Brazil. Abstracts and Excursions: pp 89–117

Eckstrand OR (1975) The Dumont serpentinite: a model for control of nickeliferous opaque mineral assemblages by alteration reactions in ultramafic rocks. Econ Geol 70: 183–201

Evans BW (1977) Metamorphism of Alpine peridotite and serpentinite. Ann Rev Earth Planet Sci 5: 397–447

Evstigneeva TL, Kudryavtsev AS, Rudashevskii NS (1992) Minerals of the platinum-group elements from Yubdo (Ethiopia): new data. Mineral Zhurn 14: 29–41 (in Russian)

Ferrario A, Garuti G (1988) Platinum-group minerals in chromite-rich horizons of the Niquelandia Complex (Central Goias, Brazil). In: *Prichard HH, Potts PJ, Bowles JFW, Cribb SJ* (eds) Geoplatinum 87. Elsevier, Amsterdam New York, pp 199–210

Ferreira FJF, Almeida Filho R, da Silva FV (2003) Modelagem de dados aeromagnéticos para estimar largura e espessura do complexo mafico/ultramafico de Campo Formoso BA. Boletim Paranaense de Geociências 52: 41–47

Garuti G (1991) Platinum-group element mineralogy and concentrations in variably altered chromitites from Niquelandia and Campo Formoso (Brazil). CSIRO, 6th Intern. Platinum Symposium, Perth (Australia). Program and Abstracts: pp 20–21

Garuti G, Zaccarini F (1997) In-situ alteration of platinum-group minerals at low temperature: evidence from chromitites of the Vourinos complex (Greece). Can Mineral 35: 611–626

Garuti G, Zaccarini F, Cabella R, Fershtater G (1997) Occurrence of an unknown Ru-Os-Ir-Fe oxide in the chromitites of the Nurali ultramafic complex, southern Urals, Russia. Can Mineral 35: 1431–1440

Garuti G, Zaccarini F, Moloshag V, Alimov V (1999) Platinum-Group minerals as indicator of sulfur fugacity in ophiolitic upper mantle: an example from chromitites of the Ray-Iz ultramafic complex (Polar Urals, Russia). Can Mineral 37: 1099–1115

Garuti G, Zaccarini F, Cabella R, Fershtater G (1998) Origin of ruthenium, osmium, iridium and iron oxides by progressive desulfidation and oxidation of laurite in Nurali chromitites (Russia). IMA 17th general meeting, Toronto, Canada, 9–14 August 1998, Abstract, A8

Lord RA, Prichard HM, Sá JHS, Neary CR (2004) Chromite geochemistry and PGE fractionation in the Campo Formoso complex and Ipuera-Medrado Sill, Bahia State, Brazil. Econ Geol 99: 339–363

Melcher F, Grum W, Simon G, Thalhammer TV, Stumpfl EF (1997) Petrogenesis of the ophiolitic giant chromite deposits of Kempirsai, Kazakstan: a study of solid and fluid inclusions in chromite. J Petrol 38: 1419–1458

Merkle RKW (1992) Platinum-group minerals in the middle group of chromitite layers at Marikana, western Bushveld Complex: indications for collection mechanism and post-magmatic modification. Can J Earth Sci 29: 209–221

Naldrett AJ, Duke JM (1980) Pt metals in magmatic sulfide ores. Science 208: 1417–1424

Oberthür T (2002) Platinum-group element mineralization of the Great Dyke, Zimbabwe. In: *Cabri LJ* (ed) The geology, geochemistry, mineralogy and mineral beneficiation of Platinum-group elements. Canadian Institute of Mining, Metallurgy and Petroleum Spec 54: 483–506

Page NJ, Zientek ML, Czamanske GK, Foose MP (1985) Sulfide mineralization in the Stillwater complex and underlying rocks. In: *Czamanske GK, Zientek ML* (eds) The Stillwater Complex, Montana: geology and guide. Montana Bureau of Mines Spec Pub 92: 93–96

Pan P, Wood SA (1994) Solubility of Pt and Pd sulfides and Au metal in aqueous bisulfide solutions. Mineral Deposita 29: 373–390

Prichard HM, Ixer RA, Lord RA, Maynard J, Williams N (1994) Assemblages of platinum-group minerals and sulfides in silicate lithologies and chromite-rich rocks within the Shetland ophiolite. Can Mineral 32: 272–294

Roeder PL (1994) Chromite: from the fiery rain of chondrules to the Kilauea Iki lava lake. Can Mineral 32: 729–746

Rudashevsky NS, Avdontsev SN, Dneprovskaya MB (1992) Evolution of PGE mineralization in hortonolitic dunites of the Mooihoek and Overwacht pipes, Bushveld Complex. Mineral Petrol 47: 37–54

Stockman HW, Hlava PF (1984) Platinum-group minerals in Alpine chromitites from southwestern Oregon. Econ Geol 79: 491–508

Stowe CW (1994) Compositions and tectonic settings of chromite deposits through time. Econ Geol 89: 528–546

Stumpfl EF (1961) Some new platinoid-rich minerals, identified with the electron microanalyser. Mineral Mag 32: 833–847

Stumpfl EF (1974) The genesis of platinum deposits: further thoughts. Minerals Sci Engng 6: 120–141

Talkington RW, Watkinson DH, Whittaker PJ, Jones PC (1984) Platinum-group minerals and other solid inclusions in chromite of ophiolitic complexes: occurrence and petrological significance. Tschermaks Mineral Petrogr Mitt 32: 285–301

Tarkian M, Stumpfl EF (1975) Platinum mineralogy of the Driekop mine, South Africa. Mineral Deposita 10: 71–85

Thompson JFH, Barnes SJ, Duke JM (1984) The distribution of nickel and iron between olivine and magmatic sulfides in some natural assemblages. Can Mineral 22: 55–66

Xiong Y, Wood SA (2000) Experimental quantification of platinum-group elements with special reference to porphyry copper environs. Mineral Petrol 68: 1–28

Zaccarini F, Garuti G, Cawthorn RG (2002) Platinum-Group Minerals in chromitite xenoliths from the Onverwacht and Tweefontain ultramafic pipes, Eastern Bushveld complex, South Africa. Can Mineral 40: 481–497

Zaccarini F, Pushkarev E, Fershatater G, Garuti G (2004) Composition and mineralogy of PGE-rich chromitites in the Nurali lherzolite-gabbro complex, southern Urals. Can Mineral 42: 545–562

Zaccarini F, Garuti G, Martin RF (2005a) Exotic accessory minerals in layered chromitites of the Campo Formoso complex (Brazil). Mitt Österr Mineral Ges 151: 125

Zaccarini F, Proenza JA, Ortega-Gutierrez F, Garuti G (2005b) Platinum Group Minerals in ophiolitic chromitites from Tehuitzingo (Acatlan Complex, Southern Mexico): implications for postmagmatic modification. Mineral Petrol 84: 147–168

Zientek ML, Cooper RW, Corson SR, Geraghty EP (2002) Platinum-group element mineralization in the Stillwater complex, Montana. In: *Cabri LJ* (ed) The geology, geochemistry, mineralogy and mineral beneficiation of Platinum-group elements. Canadian Institute of Mining, Metallurgy and Petroleum. Spec 54: 459–481

Authors' addresses: Prof. *G. Garuti* (corresponding author; e-mail: garutig@unimore.it), Department of Earth Sciences, University of Modena and Reggio Emilia, S. Eufemia 19, 41100 Modena, Italy; Prof. *J. A. Proenza*, Departament de Cristallografia, Mineralogia i Dipòsits Minerals, Facultat de Geologia, Universitat de Barcelona, C/Martí i Franquès s/n, 08028 Barcelona, Spain; *F. Zaccarini*, Department of Applied Geological Sciences and Geophysics, University of Leoben, P. Tunner Straße 5, A 8700 Leoben, Austria